

Ministry of Higher Education &
Scientific Research
Al-Nahrain University
College of Engineering



PERFORMANCE ENHANCEMENT OF OPTICAL DATA CENTERS USING SPACE-DIVISION MULTIPLEXING TECHNIQUES

A Thesis
Submitted to the College of Engineering of
Al-Nahrain University in Partial Fulfillment
of the Requirements for the Degree of Master of Science

in
Computer Engineering

by

Sarah Kareem Salim

(B.Sc. in Computer Engineering 2009)

Dhu'l-Qi'dah

1441

July

2020

Supervisor Certification

I certify that this thesis entitled "**Performance Enhancement of Optical Data Centers Using Space-Division Multiplexing Techniques**" was prepared under my supervision at College of Engineering / Al-Nahrain University in partial fulfillment of the requirements for the degree of **Master of Science in Computer Engineering**.



Prof. Dr. Raad Sami Fyath

Supervisor

10/8/2020

In view of the available recommendation, I forward this thesis for debate by the **Examining Committee**.



Dr. Aymen J. Salman

Head of the Computer Engineering Department

17/9/2020

Committee Certificate

We certify, as an Examining Committee, that we have read this thesis entitled "Performance Enhancement of Optical Data Centers Using Space-Division Multiplexing Techniques" and examined the student "Sarah Kareem Salim" in it's content and what related to it, and found it adequate for the standard of a thesis for the degree of Master of Science in Computer Engineering.



Prof. Dr. Ghassan Hamid Abdul Majid

(Chairman)

18/8/2020



Asst. Prof. Dr. Anwaar A. Al Dergazly

(Member)

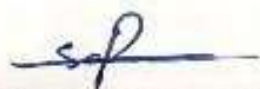
10/8/2020



Dr. Israa Badr Al-Mashhadani

(Member)

10/8/2020

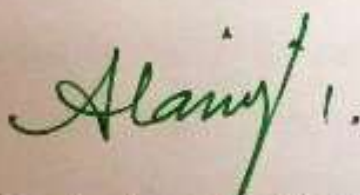


Prof. Dr. Raad Sami Fyath

(Supervisor and Member)

10/8/2020

Approved by the College of Engineering / Al-Nahrain University



Asst. Prof. Dr. Arshad AbdulJabbar Alanizi

Dean of the College of Engineering

20/9/2020

ABSTRACT

Recently, there is an increasing interest in the design of high-capacity optical interconnects (OICs) for data centers to deal with the exponential growth of traffic demand associated with advanced multimedia and internet of things (IoT) applications. The design should incorporate different multiplexing techniques to achieve terabit per second (Tbps) transmission. This thesis addresses the challenges facing the design of Tbps OICs based on combining multicore fiber (MCF) space-division multiplexing (SDM) and wavelength-division multiplexing (WDM) techniques.

A MCF-based SDM optical interconnect is designed and built in VPIphotonics 9.8 software environment. Each fiber core supports the transmission of WDM system with each channel operated with dual-polarization (DP) 16-quadrature amplitude modulation (QAM) format. The effect of intercore crosstalk on the transmission performance of the OIC is investigated under various link parameters, namely number of cores N_c , number of WDM channels per core N_{ch} , bit rate per channel R_b , and fiber length. Simulation results are reported for $R_b = 320$ and 640 Gbps, $N_c = 7$ and 19 , and N_{ch} up to 96 . The results reveal that 10 -km and 5 -km 19 -core OICs can support the transmission of 96 -channel WDM system per core operating with $R_b = 320$ and 640 Gbps respectively, when the crosstalk level is kept below -20 dB,. This leads to about 580 and 1160 Tbps transmission capacity, respectively. The investigation is then extended for longer OICs designed with loss-compensated multi-span MCF. The results reveal that nonlinear fiber optics degrade the transmission performance when the OIC length and number of WDM multiplexed channels N_{ch} are large and therefore the transmitter laser power should be optimized to achieve maximum reach.

List of Contents

| Contents | Page |
|---------------------------------------------------------------------------------------------|------|
| Abstract | I |
| List of Contents | II |
| Notations | V |
| List of Tables | X |
| List of Figures | XI |
| CHAPTER ONE: Introduction | |
| 1.1 Motivation | 1 |
| 1.2 Overview of Optical Data Center Interconnects | 3 |
| 1.3 Literature Survey | 5 |
| 1.4 Aim of The Work | 9 |
| 1.5 Thesis Organization | 9 |
| 1.6 Contributions and Limitations | 9 |
| 1.6.1 Contributions | 9 |
| 1.6.2 Limitations | 10 |
| CHAPTER TWO: High Capacity Optical Data Center Interconnects | |
| 2.1 Introduction | 11 |
| 2.2 Pulse Propagation in Single-Core Fiber Interconnect | 11 |
| 2.3 High-Capacity Optical Interconnects | 14 |
| 2.3.1 High-Order Modulation Format | 15 |
| 2.3.2 Dual-Polarization Multiplexing | 15 |
| 2.3.3 Wavelength-Division Multiplexing | 16 |
| 2.3.4 Space-Division Multiplexing | 17 |
| 2.4 Optical Space Division Multiplexing Techniques | 18 |
| 2.4.1 Multi-Mode Fiber | 19 |
| 2.4.2 Multi-Core Fiber | 20 |
| CHAPTER THREE: Design Issues and Configuration for Tbps MCF-SDM Optical Interconnect | |

| | |
|--------------------------------------------------------------------------------|-----|
| 3.1 Introduction | 25 |
| 3.2 Design Concepts for SDM-WDM-DP Interconnect | 25 |
| 3.2.1 Design Guidelines | 25 |
| 3.2.2 System Configuration | 29 |
| 3.2.2.1 Optical SDM-WDM Transmitter | 29 |
| 3.2.2.2 Optical SDM-WDM Receiver | 32 |
| 3.3 Performance of a Single-Core Optical Interconnect | 37 |
| 3.4 Calculating of Intercore Crosstalk | 44 |
| CHAPTER FOUR: Simulation Results for MCF-Based SDM Optical Interconnect | |
| 4.1 Introduction | 49 |
| 4.2 Simulation of (7, 24, 320) Interconnect | 49 |
| 4.2.1 Remarks Related to the Simulated System | 49 |
| 4.2.2 Transmission Performance of (7, 24, 320) OIC | 50 |
| 4.2.3 Effect of System Parameters | 55 |
| 4.2.3.1 Effect of Laser Linewidth | 55 |
| 4.2.3.2 Effect of Booster Amplifier Gain | 56 |
| 4.3 Effect of Number of Channels, Number of Cores, and Bit Rate | 56 |
| 4.3.1 (N_{ch} , N_c , 320) OIC | 56 |
| 4.3.2 (N_{ch} , N_c , 640) OIC | 57 |
| 4.3.2.1 7-Core OIC | 58 |
| 4.3.2.2 19-Core OIC | 60 |
| 4.4 Effect of Fiber Nonlinear Optics | 64 |
| CHAPTER FIVE: Conclusions and Suggestions for Future Work | |
| 5.1 Conclusions | 69 |
| 5.2 Suggestions for Future Work | 70 |
| REFERENCES | 73 |
| APPENDICES | |
| Appendix A | A-1 |

Notations

| Symbols | Notations |
|-------------------|---------------------------------------------|
| A | Electric field amplitude |
| A_{eff} | Effective fiber-core area |
| a_{LO} | Amplitude of the local oscillator field |
| a_s | Amplitudes of the cosine (I) of the carrier |
| B_{Link} | Optical bandwidth of the link |
| B_{me} | Electrical message bandwidth |
| B_{mo} | Optical message bandwidth |
| b_s | Amplitudes of the sine (Q) of the carrier |
| c | Speed of light in free space |
| CT | Intercore crosstalk |
| C_p | Core pitch |
| D | Group-velocity dispersion |
| Δf | Channel spacing |
| G_b | Optical booster amplifier gain |
| h | Power leakage |
| I | Optical power intensity |
| I_{PD} | photodiode current |

| | |
|-------------------|----------------------------------------------------|
| I_{BPR} | Photocurrent of the balanced photoreceiver |
| k | Coupling coefficient |
| L | Fiber length |
| L_{\max} | Maximum transmission reach |
| M | Modulation order |
| N_c | Number of cores |
| N_{ch} | Number of wavelength-division multiplexed channels |
| N_{span} | Number of spans |
| n | Fiber-core refractive index |
| n_a | Number of adjacent cores |
| n_0 | Fiber-core linear refractive index |
| n_2 | Fiber-core nonlinear refractive index coefficient |
| P_{LT} | Transmitter laser power |
| R | Bending radius |
| R_b | Data bit rate |
| R_{bT} | Total transmitted bit rate |
| R_s | Symbol rate |
| \mathcal{R} | Photodiode responsivity |
| r | Raised-cosine roll-off factor |
| S | Fiber dispersion slope |
| α | Linear power attenuation constant |

| | |
|-----------|-----------------------------------------|
| β_2 | Second-order fiber dispersion parameter |
| β_3 | Third-order fiber dispersion parameter |
| γ | Fiber nonlinearity parameter |
| λ | Optical wavelength |
| ω | Optical radian frequency |

Abbreviations

| | |
|------------|------------------------------------------------------------------------------------|
| BER | Bit Error Rate |
| BER_{th} | Bit Error Rate Threshold |
| CD | Chromatic Dispersion |
| CFR | Carrier Frequency Recovery |
| CPF | Carrier Phase Recovery |
| CW | Continuous Wave |
| DCF | Dispersion-Compensation Fiber |
| DCN | Data Center Network |
| DEMUX | Demultiplexer |
| DSP | Digital Signal Processing |
| DP | Dual Polarization |
| FEC | Forward Error Correcting Code |
| GVD | Group-Velocity Dispersion |
| HMCF | Homogeneous Multicore Fiber |
| HOM | High-Order Modulation |
| I | In-phase |
| ITU-T | International Telecommunication Union- Telecommunication Standardization Sector |
| LO | Local Oscillator |
| MCF | Multicore Fiber |

| | |
|------|----------------------------------|
| MCFA | Multicore Fiber Amplifier |
| MIMO | Multi-Input Multi-Output |
| MMF | Multimode Fiber |
| MUX | Multiplexer |
| OA | Optical Amplifier |
| OIC | Optical Interconnect |
| PBS | Polarization Beam Splitter |
| PBC | Polarization Beam Combiner |
| PD | Photodiode |
| PMD | Polarization-Mode Dispersion |
| Q | Quadrature-phase |
| SDM | Space-Division Multiplexing |
| SMF | Single-Mode Fiber |
| TDM | Time-Division Multiplexing |
| TDE | Time-Domain Equalizer. |
| WDM | Wavelength-Division Multiplexing |

List of Tables

| Table | Title | Page |
|-------|-------------------------------------------------------------------------------------------------------------------------------------------------------------------------------------------------------------------------------------------------------------------------|------|
| (1-1) | Summary of the related work concerning the use of SDM in OICs operation. NRZ: non-return-to-zero, OOK: on-off keying, DP-QPSK: dual polarization and quadrature phase-shift-keying, PAM4: 4-level pulse amplitude modulation, PAM8: 8-level pulse amplitude modulation. | 8 |
| (2-1) | Total transmission bit rate of SDM-OIC designed with MCF and assuming DP-16QAM signaling. | 18 |
| (3-1) | Total transmission bit rate for 7- and 19-core MCFs as a function of channel bit rate and number of multiplexed channels. | 28 |
| (3-2) | Parameters values used in the simulation. | 38 |
| (3-3) | L_{0dB} and $L_{critical}$ values correspond to four homogeneous MCF forms, constructed with different C_p and R . | 47 |
| (3-4) | Fiber lengths corresponding to various crosstalk levels. | 48 |
| (4-1) | Effect of transmitter laser power on BER for (7, 24,320) 10 km interconnect. | 54 |
| (4-2) | Maximum allowable crosstalk $(CT)_{max}$ as a function number of multiplexed channels for a 7-core OIC operating with $R_b = 640$ Gbps. | 60 |
| (4-3) | Dependence of $(P_{LT})_{min}$ and $(P_{LT})_{opt}$ on number of cores for 24-channel per core, 320 Gbps, DP 16-QAM channel signaling, three 100 km spans, and $N_{ch} = 24$ OIC. | 67 |

List of Figures

| Figure | Title | Page |
|--------|-----------------------------------------------------------------------------------------------------------------------------------------------------------------------------------------------|------|
| (1-1) | Transmission capacity per optical fiber in research and commercial systems [3]. | 2 |
| (1-2) | Data center interconnect applications categories. | 4 |
| (2-1) | Ways to modulate and multiplex channels to increase system capacity in optical transmission [25]. | 14 |
| (2-2) | 16-QAM constellation diagrams. (a) ideal at the transmitter side (b) example at the receiver side. | 15 |
| (2-3) | Concepts of wavelength-division multiplexing (WDM) communication system. | 16 |
| (2-4) | Types of optical fibers used in optical communication. The core diameter of SMF and MMF are around (80-10 μm) and (50-100 μm), respectively. | 19 |
| (2-5) | Principle of multimode-based space division multiplexing. | 21 |
| (2-6) | Principle of multicore fiber. | 22 |
| (2-7) | Cross-sections of seven-core MCF. | 22 |
| (2-8) | Example of homogeneous multicore fiber. | 23 |
| (2-9) | Crosstalk between the neighbor cores in MCF. | 24 |
| (3-1) | Block diagrams related to SDM-WDM data center interconnect (a) SDM-WDM transmission link (b) SDM-WDM transmitter (c) core WDM transmitter (d) SDM-WDM receiver (e) core WDM receiver. | 30 |
| (3-2) | Block diagrams of optical DP-QAM system (a) transmitter (b) receiver. | 33 |
| (3-3) | BER versus power laser transmitter for a single-core fiber carrying a single channel for different number of link spans (a) $N_{span}=2$ (b) $N_{span}=3$ (c) $N_{span}=4$ (d) $N_{span}=5$. | 39 |
| (3-4) | Variation of BER with transmission length in the absence of booster amplifier. | 41 |
| (3-5) | Maximum reach versus transmitter power laser for 320 Gbps DP 16-QAM single-core single-channel OIC. | 42 |
| (3-6) | Effect of number of WDM multiplexed channels on maximum reach for 320 Gbps DP 16-QAM single-core single-channel OIC. (a) 16-channel (b) 24-channel (c) 96-channel | 43 |
| (4-1) | Optical spectra and constellation diagrams related to (7, | 51 |

| | | |
|--------|----------------------------------------------------------------------------------------------------------------------------------------------------------------------------------------------------------------------------------------------------------------------------------------------------------------------------------------------------------------------------------|----|
| | 24, 320) OIC operating with -20 dB crosstalk (a) unmodulated WDM optical carriers (b) amplified SDM-WDM transmitter signal (c) optical signal after 10 km transmission (d) intercore crosstalk signal (e) constellation diagrams corresponding to Ch13 received in three different cores (core1, core5, and core7). | |
| (4-2) | Variation of BER with intercore crosstalk for (7, 24, 320) OIC after 10 km transmission. | 53 |
| (4-3) | Dependence of BER of (7, 24, 320) OIC operating with -20 dB crosstalk on laser linewidth after turning ON the (CFR+CPR) unit. | 55 |
| (4-4) | Effect of booster amplifier gain on the maximum transmission distance during absence of crosstalk and presence of -20 dB crosstalk for (7, 24, 320) OIC. | 57 |
| (4-5) | Optical spectra and constellation diagrams related to (7, 24, 640) system operating with -20 dB crosstalk (a) unmodulated WDM optical carriers (b) amplified SDM-WDM transmitter signal (c) optical signal after 10 km transmission (d) intercore crosstalk signal (e) constellation diagrams corresponding to Ch13 received in three different cores (core1, core5, and core7). | 58 |
| (4-6) | Variation of BER with number of multiplexed channels for 19-core, 10 km OIC operating with $R_b = 640$ Gbps. | 61 |
| (4-7) | Variation of BER with transmission length for (19, 24, 640) OIC operating with -20 dB crosstalk. | 62 |
| (4-8) | Optical spectra and constellation diagrams related to (19, 96, 640) OIC operating with -20 dB crosstalk (a) unmodulated WDM optical carriers (b) amplified SDM-WDM transmitter signal (c) optical signal after 5km transmission (d) intercore crosstalk signal (e) constellation diagrams corresponding to Ch49 received in three different cores (core1, core9, and core19). | 63 |
| (4-9) | Dependence of BER on the power laser transmitter when 320 Gbps, DP 16-QAM channel signaling, three 100 km spans, and $N_{ch} = 24$ are assumed for (a) 7-core OIC.(b) 19-core OIC (c) 37-core OIC. | 65 |
| (4-10) | Variation of BER with transmitter power laser for 3×100 km, 7-cor, $R_b = 320$ Gbps, and $N_{ch} = 24$ OIC operating in the absence of nonlinearity. | 68 |

CHAPTER ONE

Introduction

1.1 Motivation

Recently, there is an exponential increase in data traffic demand to cooperate with advanced applications such as Internet of Things (IoT), 5G network services, and three-dimensional video transmission. This increasing demand stands as one of the main challenges facing advanced optical communication systems [1] and optical networks [2]. The current optical transmission systems are based on different enabling technologies, such as time-division multiplexing (TDM), wavelength-division multiplexing (WDM), and digital coherent technology using digital signal processing (DSP). An overview of capacity growth per fiber across the years is depicted in Fig.1-1 [3]. The transmission capacity per fiber has reached 100 Tbps in research, and 10 Tbps in commercial systems. The above three major technologies have led to increases in optical fiber transmission capacity by a factor of more than 10^5 times over the past three decades. As the capacity grows at an annual rate of 1.4 times, and is predicted to grow at an even faster rate, research and development continues to target larger capacity. However, around the year 2020, transmission capacity will supposedly reach the theoretical limit over a single-mode fiber (SMF) of around 100 Tbps [3]. Today's optical systems have already implemented solutions on all the available degrees of modulation freedom (namely: polarization, frequency, phase, and amplitude). In fact the only unused dimension is space. Space-division multiplexing (SDM) technique opens a new degree of freedom to enhance the capacity of the optical transmission link by multiplexing the data

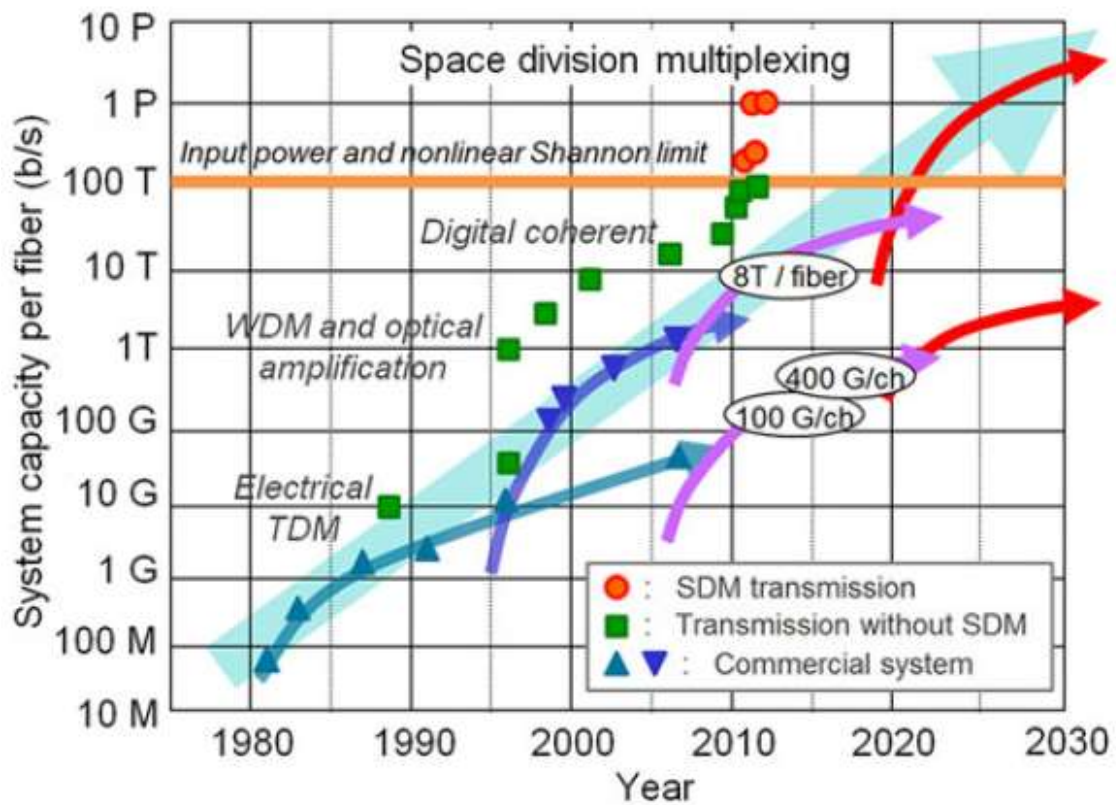


Figure 1-1 Transmission capacity per optical fiber in research and commercial systems [3].

in the modes of a multimode fiber [4], cores of multi single-mode core fiber [5], or a hybrid of both multiplexing schemes [6].

To deal with this increasing traffic requirement, the new advanced optical networks generally operate with hybrid multiplexing techniques based on a combination of WDM and dual-polarization (DP) transmission (i.e., polarization multiplexing) [7] and supported by SDM [8]. The performance of optical communication systems and optical networks incorporating SDM technique may be degraded due to the presence of intermodal or/and intercore crosstalk. Multicore fiber (MCF) crosstalk requirements per unit length are fairly independent of the transmission distance in the context of modern coherent optical communication systems [9].

Future Tbps data center optical interconnects (OICs) are expected to be designed with a hybrid multiplexing technique based on MCF-SDM and WDM. The transmission performance of these interconnects should be addressed carefully for various system parameters such as transmission bit rate, number of fiber cores, and number of WDM channels. The major distance limitation may come from intercore crosstalk. These issues will be addressed in this thesis.

1.2 Overview Optical Data Center Interconnect

Over the last few years, the exponential increase of the Internet traffic, essentially driven from emerging applications (e.g., social networking, streaming video, and cloud computing) has formed the requirement for more robust warehouse data centers. These data centers are based on thousands of high performance servers interconnected with high performance switches. The applications that are hosted in the data center servers (e.g., cloud computing applications, search engines, etc.) are extremely data intensive and require high interaction between the servers in the data center. This interaction creates the need for high bandwidth and low latency communication networks between the servers in the data centers. Furthermore, these data centers must comply with low power consumption requirements in order to reduce the total operating cost [10]. As a result, a scalable and efficient infrastructure for data center networks (DCNs) are required. Optical interconnects supported by high-order modulation and multiplexing techniques could provide a perfect solution for this challenge. The OICs between data centers could span anywhere from tens of kilometer of terrestrial distances to thousands of kilometer of subsea routes. There are two main data center interconnects [11] as shown in Fig. 1-2

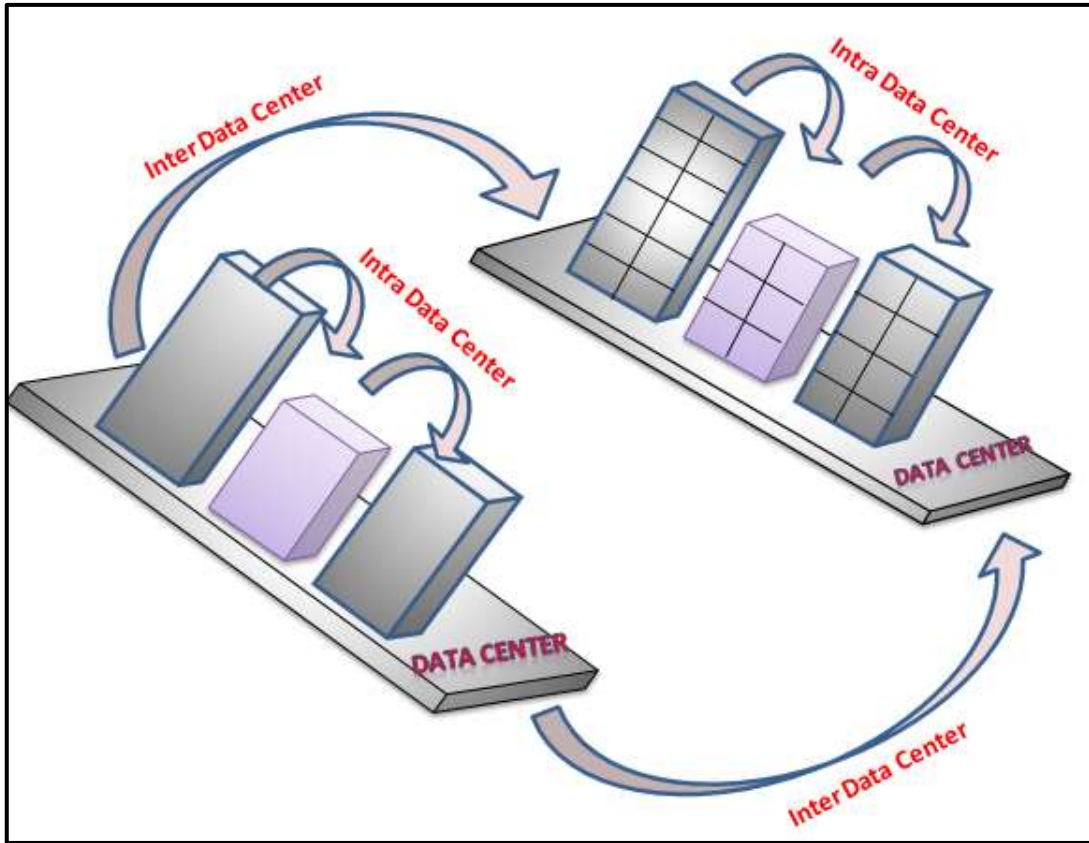


Figure 1-2 Data center interconnect applications categories.

- i. Intra-Data Center Interconnect: Intra-data center interconnect means connections within the data center. It can be within one building or between data center buildings on a campus. Connections can be a few meters up to 10 km.
- ii. Inter-Data Center Interconnect: Connections between data centers from 10 km up to 80 km. Of course, connections can be much longer but most of the market activity for inter-data center connect is focused on 10 km to 80 km, longer connections are considered metro or long haul.

Optical interconnects seem as a promising solution for the DSN offering high bandwidth, low latency and reduced energy consumption. Several schemes have been presented for the exploitation of the light's high

bandwidth such as WDM. In the case of WDM, using separate wavelengths that can travel simultaneously in the fiber providing significantly higher bandwidth. The current demand for supporting data center applications has been posing stringent requirements on short-reach transmission techniques. To address the high capacity demand in DCNs, scaling up the fiber capacity by SDM approach has been proposed to boost the single fiber capacity [12].

1.3 Literature Survey

In 2017, Butler et al. [13] assembled and tested short reach SDM fiber transmission systems with up to 2 km distance using MCF. Systems with combinations of various fibers, fan-outs cabling and connectors were investigated. The results show that low loss and crosstalk were achieved on MCF of 2 and 8 cores. Moreover, penalty-free bit error rate was obtained from system operating with 0.2 km of 8-core fiber with fan-outs and up to 2 km in dual-core fiber.

In 2018, Yuan et al. [14] evaluated the benefits of MCF-based SDM evaluations in term of maximizing the capacity and spatial efficiency of DSNs. An analytical model for intercore crosstalk (CT) in bidirectional normal step-index and trench-assisted MCFs was presented. A CT-aware core prioritization scheme was proposed. CT-aware spectrum resource allocation strategies were also developed to relieve the complexity of the CT-computation. Several combinations of core mapping and spectrum allocation algorithm were investigated for eight types of homogenous MCFs comprising 7-61 cores, three different multiplexing schemes, and DSN topologies.

In 2018, Yuan et al. [15] derived a wavelength-dependent crosstalk calculation formula for bi-directional homogeneous MCFs with nonidentical

core pitches. They showed that highly dense 61-core hexagonal and 52-core rectangular MCFs are the perfect candidates for small scale data centers with few meter link distances. The 37-core hexagonal MCF achieved best results for intra-cluster network and 19-core hexagonal MCFs can be utilized for larger multi-cluster data centers.

In 2018, Yan et al. [16] investigated the relation between the blocking and throughput in modular DSNs based on SDM. They combined the two metrics linearly by a weight factor that prioritizes them relatively. To solve the resource allocation problem, they proposed both mixed integer linear programming formulations and close-to-optimal heuristics for three different SDM switching schemes. The Simulation results explained that a carefully chosen weight factor is necessary to achieve a proper balance between the blocking probability and throughput for all the schemes.

In 2019, Sakaguchi et al. [6] demonstrated the feasibility of bi-directional transmission over 13 km 39-core 3-mode fiber with a total of 228 spatial channels. Aggregated intercore crosstalk was below -35 dB over C and L bands. The feasibility of the proposed system was investigated using bi-directional transmission of 10GHz band, 37.38 Gbps dual polarization-quadrature phase-shift-keying (DP-QPSK) signals at 1550 nm using coherent detection with a 6×6 multi-input multi-output (MIMO) equalizer.

In 2020, Zhang et al. [17] addressed enabling technologies for SDM-based optical DCNs and provided an overview of related interconnect architectures, components, and transmission options. The key technologies behind optical multiplexers, demultiplexers, and switches for SDM OICs were presented. The authors outlined that using high-order modulation format and WDM to support high-capacity transmission in OICs are one of the main challenges

facing SDM transmission. Furthermore, combining WDM and SDM to increase the capacity and flexibility of OICs may be a feasible approach for extending the conventional WDM counterpart with the space domain. It was stated that intercore crosstalk need to be considered for DCN links and the transmission quality degradation can be reduced by heterogeneous MCF deployment, in which this type of crosstalk can be significantly decreased.

In 2020, Mendinueta et al. [18] presented new opportunity for fast optical switching networks based on SDM and coherent burst-mode technologies for converged inter/intra data center and edge optical networks. The investigation show that MCFs with low intercore crosstalk may be used with packet spatial super- and core-joint SDM optical switches in a time-slotted network. The two fundamental components of this network are the SDM fast optical switch and the coherent burst-mode receiver. Two experiments were demonstrated for such a switching network achieving a capacity of 53.3 Tbps with 7 spatial channels and DP-QPSK and a capacity of 83.33 Tps with 8 spatial channels and DP-8PSK. Each spatial channel carries 64-wavelength WDM system. The estimated bit rate per wavelength in the spatial channel is approximately 120 and 160 Gbps, respectively. Furthermore, 7-core 2km, 19-core 10km, and 19-core 28 km were used to support the demonstration.

Summary of the related work is given in Tables 1-1. In general, these references have mentioned that the performance of MCF-based SDM OICs may be degraded due to the presence of interconnect crosstalk even for short ones. Furthermore, they have suggested to make further investigation to address the effect of OIC parameters on the transmission performance in the presence of intercore crosstalk. These issues will be addressed in this thesis.

Table 1-1 Summary of the related work concerning the use of SDM in OICs operation.

NRZ: non-return-to-zero, OOK: on-off keying, DP-QPSK: dual polarization and quadrature phase-shift-keying, PAM4: 4-level pulse amplitude modulation, PAM8: 8-level pulse amplitude modulation.

| Year Ref. | No. of Cores | No. of Core Modes | Fiber Length | Bit Rate (Gbps) | Multiplexing Type | Modulator Type | Work Type |
|--------------------------------|--------------|-------------------|--------------|-----------------|-------------------|----------------|------------------------------|
| 2017 Butler et al. [13] | 8 | 1 | 200 m | 25 | SDM | NRZ | Experimental |
| | 2 | | 2 km | | | | |
| 2018 Yuan et al. [14] | 7 | 1 | | 10 | SDM-WDM | OOK | Theoretical |
| | 19 | | | 100 | | DP-QPSK , PAM4 | |
| | 37 | | | 110 | | OOK+ PAM4 | |
| | 61 | | | 300 | | PAM8 | |
| 2018 Yuan et al. [15] | 7 | 1 | >1 km | 10 | SDM-WDM | PAM8 | Theoretical |
| | 19 | | 250-1000 m | 100 | | OOK | |
| | 37 | | 10-250 m | 110 | | DP-QPSK , PAM4 | |
| | 61 | | <10 m | 300 | | OOK+ PAM4 | |
| 2019 Sakaguchi et al. [6] | 39 | 3 | 13 km | 37.38 | SDM | DP-QPSK | Experimental |
| 2020 Mendinueta et al. [18] | 7 | 1 | | 53300 | SDM-WDM | DP-QPSK | Theoretical and experimental |
| | 8 | | | 83330 | | DP-8PSK | |

Performance investigation of SDM-based optical communication systems has also attracted researchers in Iraqi universities. Few results have been reported in the literature since the topic is relatively new. The results are limited to multimode multiplexing in a single-core fiber to address high-capacity long-haul transmission [19-21] and they are not related to datacenter interconnect.

1.4 Aim of the Work

The aim of this thesis is to enhance the transmission performance of optical data centers interconnects using SDM technique. A MCF with 7, 19, and 37 cores having-single mode will be investigated for transmission link supported by WDM technique.

1.5 Thesis Organization

The organization of this thesis is presented in five chapters including the introduction given in chapter one. Chapter two contains background of SDM with brief description of WDM and the required basics of high capacity OICs. Chapter three presents design issues and configuration for Tbps MCF-SDM OIC. Simulation Results for MCF-based SDM OICs are presented in chapter four. The main conclusions for this work are given in chapter five along with suggestions for future work.

1.6 Contributions and Limitations

1.6.1 Contributions

The main contributions of this work are

- i. A new and comprehensive model for WDM/MCF-based SDM optical interconnect has been developed in VPIphotonics software environment. The model takes into account the effect of different system parameters including number of fiber cores, number of WDM channels per core, data rate per channel, modulation formats.
- ii. A new scenario has been proposed to estimate the maximum reach of MCT-based SDM interconnects when intercore crosstalk exists.

- iii. Theoretical model has been developed to design SDM interconnects carrying Tbps data rate. This yield two new interconnects transmitting 583 and 1160 Tbps over 10 and 5km, respectively.

1.6.2 Limitations

The main limitations of this work are

- i. Scarcity of advanced optical network Lab in Iraqi universities to demonstrate the main concepts and findings of this work.
- ii. VPIphotonics software is high-cost and therefore a demo version is used to obtain the simulation results.

CHAPTER TWO

High Capacity Optical Data Center Interconnects

2.1 Introduction

Background topics related to the work being concluded in this thesis are presented in this chapter. A brief overview of pulse propagation in single-core fiber interconnects is given to introduce the main optical physical parameters of the link. The primary concepts of amplitude quadrature modulation (QAM) and wavelength-division multiplexing (WDM) are also briefly explained. A detailed description of space-division multiplexing (SDM) technique is then outlined as a promising way of increasing the fiber transmission capacity in optical interconnect (OIC). This chapter also gives a brief picture of intercore crosstalk in multicore fiber (MCF) since it plays a key role in determining the transmission capacity of SDM-WDM OIC.

2-2 Pulse Propagation in Single-Core Fiber Interconnect

The conventional high-speed OIC is usually designed using a single-core fiber having single-mode propagation characteristics. The pulse propagation through this OIC is governed by linear mechanisms, namely attenuation and dispersion, and nonlinear mechanism coming from nonlinear fiber optics. The dynamic evolution of the propagating pulse is described by the nonlinear Schrodinger equation [22]

$$\frac{\partial A}{\partial z} + \frac{\alpha}{2}A + \frac{j\beta_2}{2}\frac{\partial^2 A}{\partial z^2} - \frac{\beta_3}{6}\frac{\partial^3 A}{\partial t^3} = j\gamma|A|^2A \quad (2.1)$$

where the OIC is assumed to be extended along the z axis. Furthermore,

A = Electric field amplitude of the pulse which is a function of distance z and time t (i.e., $A(z, t)$).

α = Linear power attenuation constant of the OIC (unit = km^{-1}).

β_2 and β_3 = Second- and third-order dispersion parameters of the OIC

γ = Nonlinear parameter of the OIC.

The OIC propagation loss comes mainly from intrinsic absorption, extrinsic absorption, and scattering. For an OIC of length L , the output power P_{out} is related to the input power P_{in} by [23]

$$P_{\text{out}} = P_{\text{in}} e^{-\alpha z} \quad (2.2)$$

The total link loss measured in decibels is given by $10 \log(P_{\text{in}}/P_{\text{out}}) = [10 \log e] \alpha L = 4.34 \alpha L$. Thus the loss parameter of the link measured in dB/km is given by

$$\alpha_{\text{dB}} = 4.34 \alpha \quad (2.3)$$

where the linear power-attenuation parameter α is measured in km^{-1} .

The dispersion in single-mode fiber (SMF) comes mainly from the material dispersion characteristics where the refractive index n of the core is frequency dependent. The parameter n affects the phase propagation constant β of the travelling wave in the link. To illustrate this, consider a wave of single-radian frequency ω is traveling across the link, then its electric field $a(z, t)$ can be expressed as [24]

$$a(z, t) = A(z, t) \cos(\omega t + \beta(\omega)z) \quad (2.4a)$$

where

$$\beta(\omega) = \frac{2\pi n(\omega)}{\lambda} = \frac{\omega n(\omega)}{c} \quad (2.4b)$$

where λ is the optical wavelength, c is the speed of light in free space. In addition, $\omega = 2\pi f$ and $f = c/\lambda$ is the optical frequency measured in Hz.

When an optical carrier of frequency ω_0 is modulated by the electrical information signal, the modulated optical spectrum generally contains different spectral components around ω_0 . Therefore, it is useful to expand $\beta(\omega)$ in Taylor series around the unmodulated carrier frequency ω_0 [22]

$$\beta(\omega) = \beta_0 + (\omega - \omega_0)\beta_1 + \frac{1}{2}(\omega - \omega_0)^2\beta_2 + \frac{1}{6}(\omega - \omega_0)^3\beta_3 + \dots \quad (2.5a)$$

where $\beta_0 \equiv \beta(\omega_0)$ and

$$\beta_m = \left(\frac{d^m \beta}{d\omega^m} \right)_{\omega = \omega_0} \quad m=1, 2, \dots \quad (2.5b)$$

The 2nd- and 3rd-order dispersion parameters β_2 and β_3 are usually expressed using engineering parameters, namely group-velocity dispersion (GVD) D and dispersion slope $S \equiv dD/d\lambda$ [23]

$$D = \frac{2\pi c}{\lambda^2} \beta_2 \quad (2.6a)$$

$$S = \left(\frac{2\pi c}{\lambda^2} \right)^2 \beta_3 + \left(\frac{4\pi c}{\lambda^3} \right) \beta_2 \quad (2.6b)$$

A signal-channel OIC usually operates at $\lambda = 1550$ or 1310 nm [25]. The 1550 nm wavelength corresponds to the minimum-attenuation wavelength of silica SMF. In this wavelength, $\alpha_{dB} = 0.2$ dB/km and $D \approx 17$ ps/(nm.km). The 1310 nm-wavelength operation is characterized by almost negligible GVD ($D \approx 0$) and relatively high loss ($\alpha_{dB} \approx 0.35$ dB/km).

The nonlinear parameter γ in eqn. 2.1 is related to Kerr effect which describes the dependence of the medium refractive index on the optical power intensity I in the medium. The refractive index of the silica fiber core depends

on the intensity of the optical wave passing through it. Under Kerr effect, $n(I) = n_0 + n_2 I$ where n_0 is the low-intensity refractive index of the silica and n_2 is its nonlinear refractive index coefficient. The parameter γ is related to n_2 by [24]

$$\gamma = \frac{\omega n_2}{c A_{eff}} \quad (2.7)$$

where A_{eff} is the core effective area of the OIC.

2.3 High-Capacity Optical Interconnects

Different ways have been reported in the literature to modulate and multiplex channels to increase the transmission capacity of OICs. These ways stand heavily on hybrid amplitude/phase modulation formats and different multiplexing techniques in the polarization, frequency, and space domains, as shown in Fig. 2-1 [25]. Brief description of these ways is given in Sections 2.3.1-2.3.4.

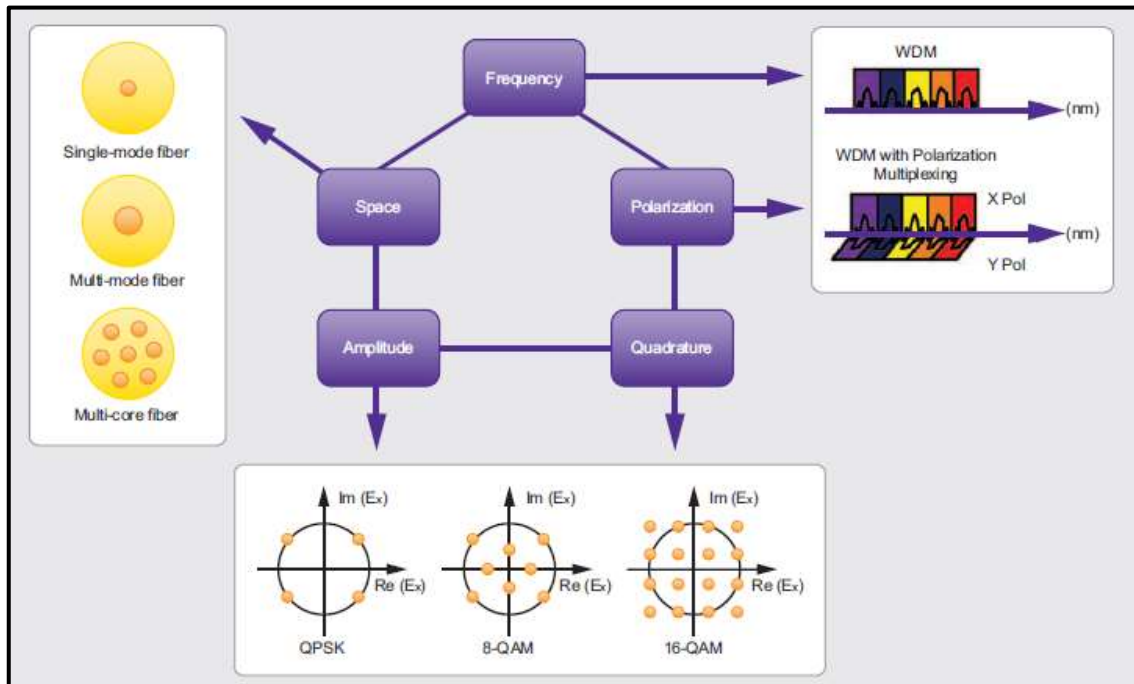


Figure 2-1 Ways to modulate and multiplex channels to increase system capacity in optical transmission [25].

2.3.1 High-Order Modulation Formats

High-order modulation (HOM) uses M discrete symbols to carry the data and each symbol has $\log_2 M$ bits [26]. For example, $M = 2$ (i.e., binary) and $M = 16$ yield 1 bit and 4 bits per symbol, respectively. Generally, M-QAM signaling is used in advanced OICs where M discrete symbols are transmitted and the data are embedded in both in-phase (I) and quadrature-phase (Q) of the carrier leading to QAM signaling. Figure 2-2 shows the constellation diagram of 16-QAM signals where each symbol carrier $\log_2 16 = 4$ bits.

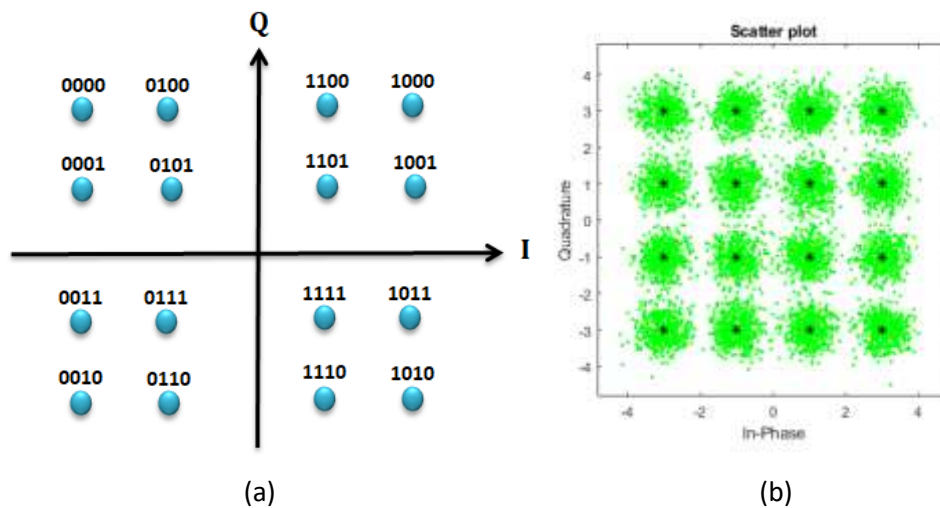


Figure 2-2 16-QAM constellation diagrams. (a) ideal at the transmitter side
(b) example at the receiver side.

2.3.2 Dual-Polarization Multiplexing

In dual-polarization (DP) multiplexing, the transmitter laser field is splitted into two orthogonally polarized components and each component is modulated by half the data. Thus DP system transmits two parallel channels

in the link leading to double the transmission bit rate compared with the single-polarization counterpart [27].

2.3.3 Wavelength-Division Multiplexing

The WDM is based on dividing the optical frequency domain into many slots and each slot is dictated to one channel. The WDM systems transmit parallel N_{ch} optical channels in parallel in the link using N_{ch} frequency-separated laser sources [7] as shown in Fig. 2-3. Therefore, the capacity of WDM system equal $N_{ch} \times$ capacity of the single channel while using the same speed of electronic interfaces. WDM-based OICs usually operate either in the C-band (1530 – 1565 nm), i.e., 1550 nm-region, or O-band (1260 – 1360 nm), i.e., 1310 nm-region.

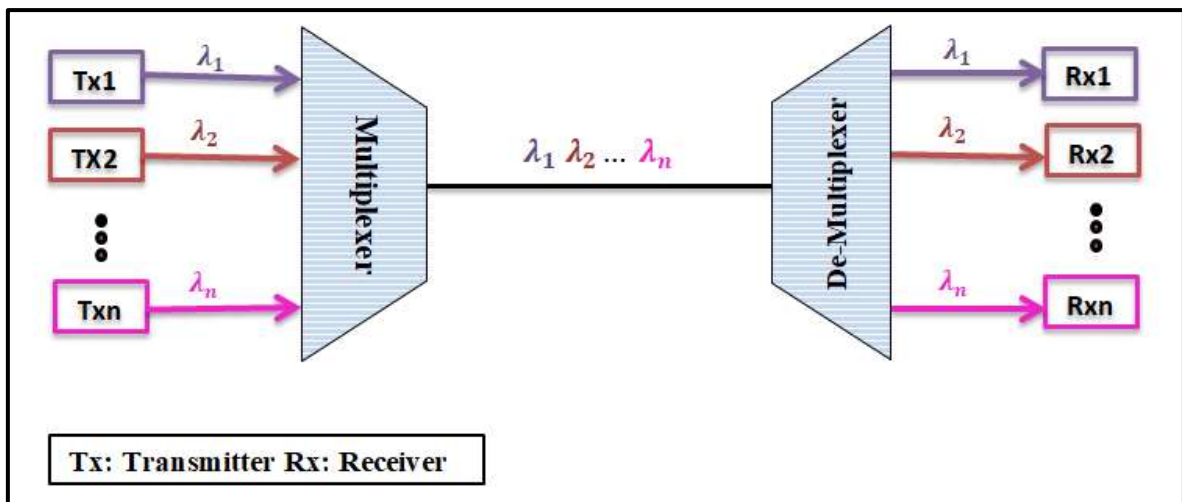


Figure 2-3 Concepts of wavelength-division multiplexing (WDM) communication system.

2.3.4 Space-Division Multiplexing

In SDM, the OIC uses the modes of multimode fiber and/or cores of multicore fiber (MCF) to enhance its transmission capacity [6, 17]. Using N_c -core fiber and each mode of them N_m modes in each core is used to carry one channel (single-or WDM system) will enhance the OIC capacity by $N_m N_c$ compared with a single-core single-mode counterpart.

The symbol rate R_s (i.e., total transmission bit rate R_{bT} divided by number of bits carried by each symbol) of advanced OICs is limited by the speed of used electronics. Symbol rates up to 50 giga symbol per second (GSps) have been already reported in many experimental and implemented links. Many research groups are working to increase R_s toward 100 GSps. Table 2-1 shows how the capacity of MCF-base SDM OIC is affected by the number of fiber cores N_c when $R_s = 50$ and 100 GSps. Each core supports a single-mode operation and carries N_{ch} -WDM system with DP-16 QAM signaling. Results are given for OICs designed with $N_c = 1, 7, 19,$ and 37 , usually used in homogeneous MCFs, and for values of $N_{ch}=48$ and 96 . Note that the product $N_{ch}N_c$ plays a key role in determining the capacity of the interconnect. When $R_s= 50$ GSps, the 10 Tbps OIC should be designed with $N_{ch}N_c= 25$. In this case, 7-core OIC operating with 4-ch WDM system per core can support the required design. The 100 Tbps OIC requires $N_{ch}N_c= 250$ and can be designed with 7-core and 36-ch WDM per core system. The 100 Tbps OIC can also be designed with 19- and 37-core fibers when each core carries 16- and 8-ch WDM systems, respectively. Note that $N_{ch} = 2^{\text{integer}}$ are usually used in WDM systems.

Table 2-1 Total transmission bit rate of SDM-OICs designed with MCF and assuming DP-16QAM signaling.

| Number of Cores | Total Transmission Bit Rate (Tbps) | | | |
|-----------------|------------------------------------|-----------|------------------|-----------|
| | $R_s = 50$ GSps | | $R_s = 100$ GSps | |
| | 48-Ch WDM | 96-Ch WDM | 48-Ch WDM | 96-Ch WDM |
| 1 | 19.2 | 38.4 | 38.4 | 76.8 |
| 7 | 134.4 | 268.8 | 268.8 | 537.6 |
| 19 | 364.8 | 729.6 | 729.6 | 1459.2 |
| 37 | 710.4 | 1420.8 | 1420.8 | 2841.6 |

2.4 Optical Space-Division Multiplexing Techniques

Nowadays the term SDM is taken to refer to multiplexing techniques that establish multiple spatially distinguishable data pathways through the same fiber. SDM emerged as a solution to the bandwidth exhaustion issue of optical transmission systems to further increase fiber efficiency or spatial capacity.

One of the basic transmission medium of the OICs for data center is a SMF, which has only one waveguide (core) supporting a single-waveguide mode operation. In optical fiber transmission, to increase the achievable data throughput and also to encourage energy and resource savings, hardware integration, and joint signal-processing, three SDM schemes have been proposed. These are [28]

- i. Mode-division multiplexing (MDM) using multimode fibers (MMFs) where a single strand of fiber has one core with sufficiently large cross-section area to transmit different signals across the single core.

- ii. Core multiplexing using MCF, by combining multiple cores within a single cladding.
- iii. Hybrid of MCF and multimode multiplexing. In this case, each core of the MCF supports multimode operation.

Types of optical fiber which are mentioned above can be seen in Fig. 2-4. The cladding diameter of SMF is about $125\ \mu\text{m}$ with a small core diameter of between $8\text{-}10\ \mu\text{m}$. Adapting the increasing number of modes in MMF; core diameter is around $50\text{-}100\ \mu\text{m}$. In MCF, the cladding diameter appears to be large typically $200\text{-}300\ \mu\text{m}$ to contain multiple cores inside. Modal dispersion in MMF and intercore crosstalk (CT) in MCF are the key challenge restricting the increase number of cores or modes in fiber, transmission distance and the sum of data it transfers [29,30].

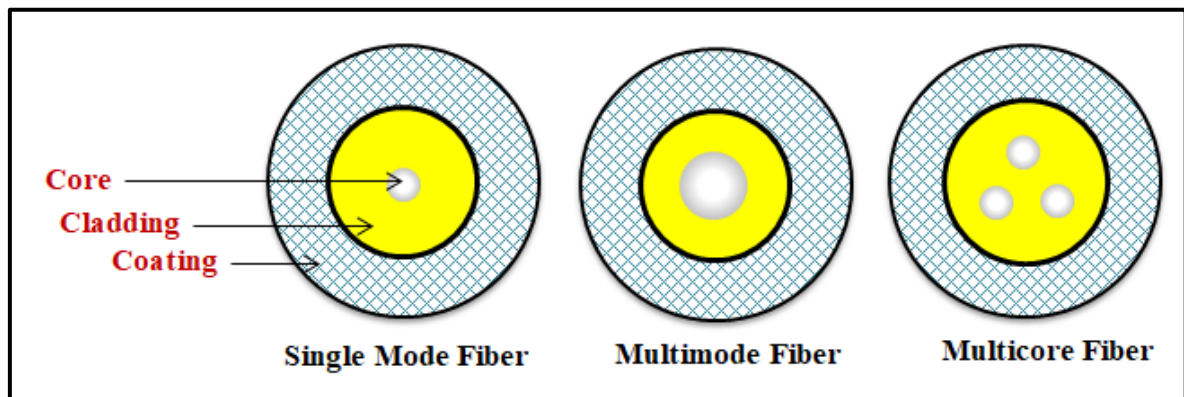


Figure 2-4 Types of optical fibers used in optical communication. The core diameter of SMF and MMF are around $(80\text{-}10\ \mu\text{m})$ and $(50\text{-}100\ \mu\text{m})$, respectively.

2.4.1 Multimode Fiber

MMF is an optical fiber which supports many of transverse guided modes. It is designed to transmit multiple light rays or modes simultaneously, each at

a slightly different angle of reflection within the data transferred optical fiber core [31]. At different angles relative to the optical fiber axis, the light rays from the source enter the fiber core. The rays entering with a smaller angle will pass through the fiber along a more direct path in comparison to rays entering with a greater angle and will reflect many more times during propagation. Thus, each mode can follow a different optical path inside the optical fiber. Consequently, the time it takes to arrive at the end of the fiber varies depending on the mode. This is known as differential mode group delay. As a result, the non-simultaneous arrival of the various signal components deforms the shape of the originally transmitted signal. The fiber's refractive index profile greatly impacts the velocity of the different propagation modes, causing modal dispersion. The way to deal with such issues is to compensate those impairments through heavy multi-input multi-output (MIMO)-digital signal processing (DSP) to separate each mode when they are received on the receiver side [32]. For the aforementioned reasons MMF operate efficiently in short distances, such as within a building or on a campus. In theory, few-mode fiber is the same as MMF but is manufactured to allow the propagation of fewer modes (2-4 modes), therefore lightening the DSP load at the receiver end and making long-distance communication possible [33]. Each of these mode carriers it is own data leading to multimode SDM as shown Fig. 2-5.

2.4.2 Multicore Fiber

MCF is a type of fibers that contains multiple cores in one common cladding as shown in Fig. 2-6. The number of cores varies inside the cladding depending on the design parameters taking into consideration. With MCFs,

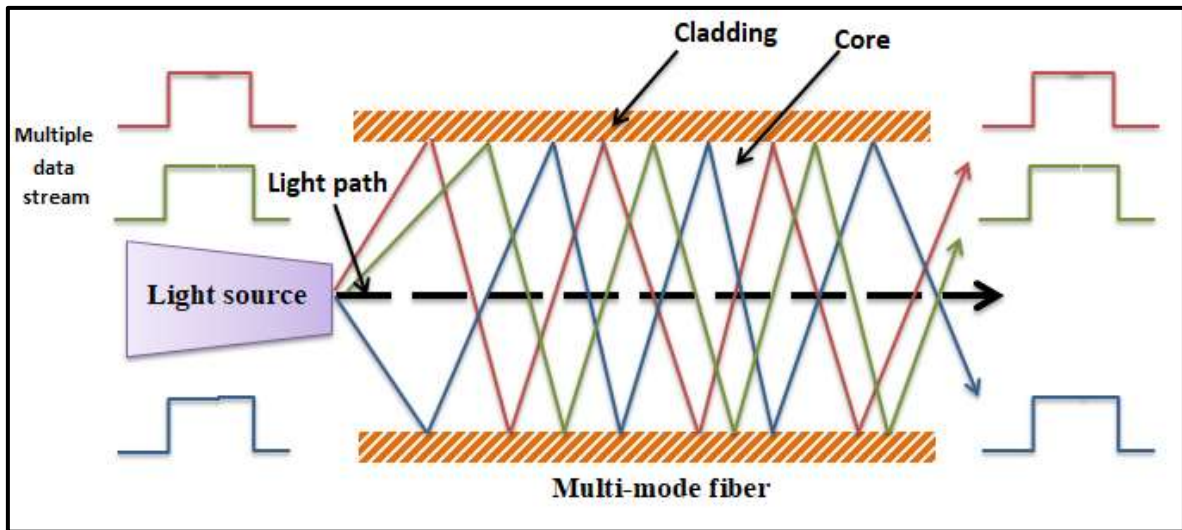


Figure 2-5 Principle of multimode-based space division multiplexing.

not only core design, but the number of cores, the core layout, the outer cladding thickness (the minimum distance between the middle of the outer cores and the cladding-coating interface), and the cladding diameter can be optimized from the optical and mechanical properties perspective [34]. Figure 2-7 exhibits seven-core MCF and it is chosen here to introduce the primary parameters considered on MCF. The configuration of this particular MCF is a core at its center and six outer cores equally separated from the center. Each core has its own diameter, the distance that separates two adjacent cores is called core pitch.

According to the core pitch, MCF is classified into two types: the uncoupled core and the coupled core. The second type allows high coupling between signals that transmit in adjacent cores, thus showing large amounts of crosstalk interference even after a few meters. In that case, receiver side usage of MIMO-DSP is inevitable [35].

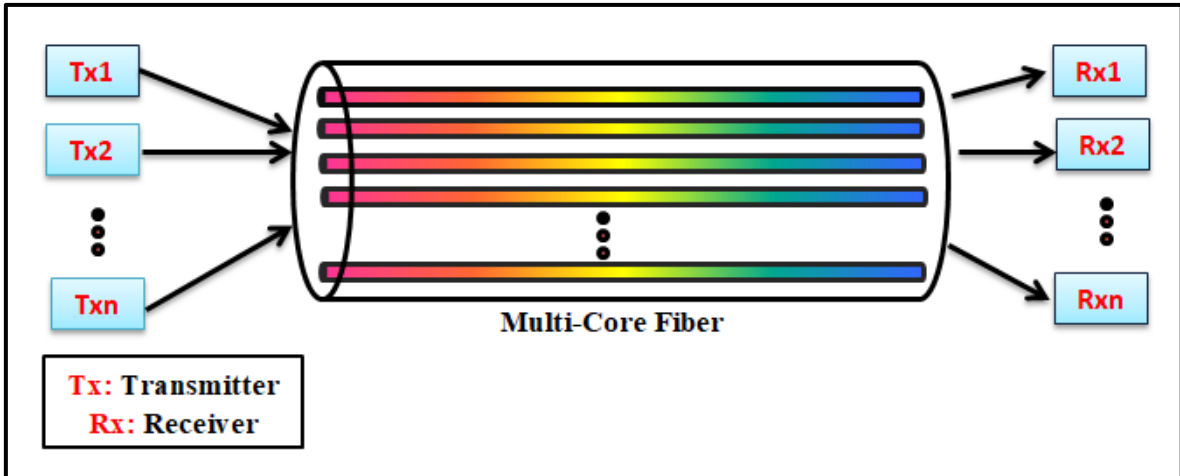


Figure 2-6 Principle of multicore fiber.

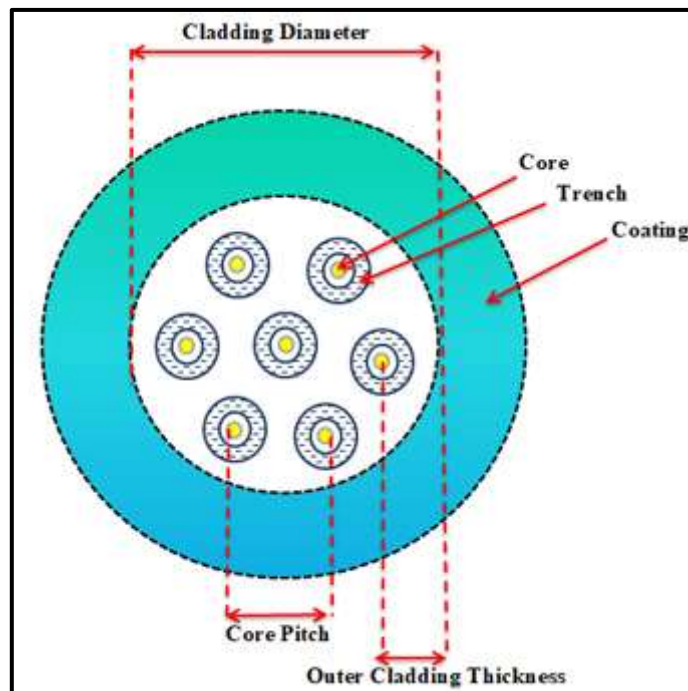


Figure 2-7 Cross-sections of seven-core MCF.

In the sense of the spatial homogeneity of the MCF structure, one can differentiate between a homogeneous MCF (HMCF) and a heterogeneous

MCF. In the first case, all cores have the same refractive index profile, while in the second case, the MCF consists of at least one core with a different refractive index profile [36, 37]. HMCF with a hexagonal arrangement is widely used in research experiments and trials. The basic characteristics of HMCF are that the core pitch between any two adjacent cores is the same following a triangle lattice and all cores are made of the same material as shown in Fig. 2-8. This kind of fiber has been described as the primary enabler of SDM systems technology.

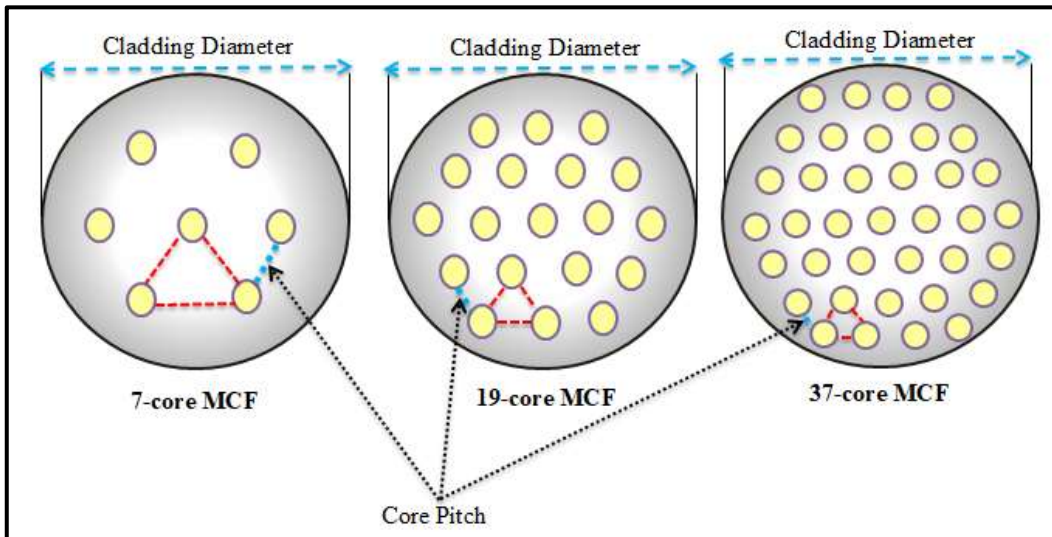


Figure 2-8 Examples of homogeneous multicore fiber.

The number of cores that can fitting in a fiber is calculated by this centered hexagonal number order series

$$\text{Number of cores} = 3 \times M \times (M - 1) + 1, \quad M = 1, 2, \dots \quad (2.8)$$

The first few hexagonal digits centered are 1, 7, 19, 37, 61, 91, 127, 169, 217 . . . [32].

The most critical limitation in MCFs is the intercore crosstalk (CT) that is the amount of "leaking" optical signal power from neighboring cores to a different one, creating interference with the already propagating signal there. The crosstalk phenomenon derives from the disparity in the number of adjacent cores closest to it [38]. Figure 2-9 shows that the inner core, which includes the largest number of neighboring cores, is suffered by the crosstalk most, whereas the outer cores contains the smallest cores and the few crosstalk, assuming that all cores have equivalent signal power. Crosstalk is produced dominantly when signals are transmitted in adjacent cores with the same wavelengths. The maximum numbers of cores and the core arrangement have to be carefully determined based on the required CT considering a modulation format to be used in the transmission and the target effective area size. BER of 10^{-3} is < 1 dB, when the crosstalk is < -18 dB for QPSK, -24 dB for 16-QAM, and -32 dB for 64-QAM [39]. MCF is considered to be the most feasible and effective way to realize SDM networks. Its implementation within data centers seems to be highly likely as the issue of CT is not serious over short link lengths (< 1 km) relative to that of long-haul transmission [14].

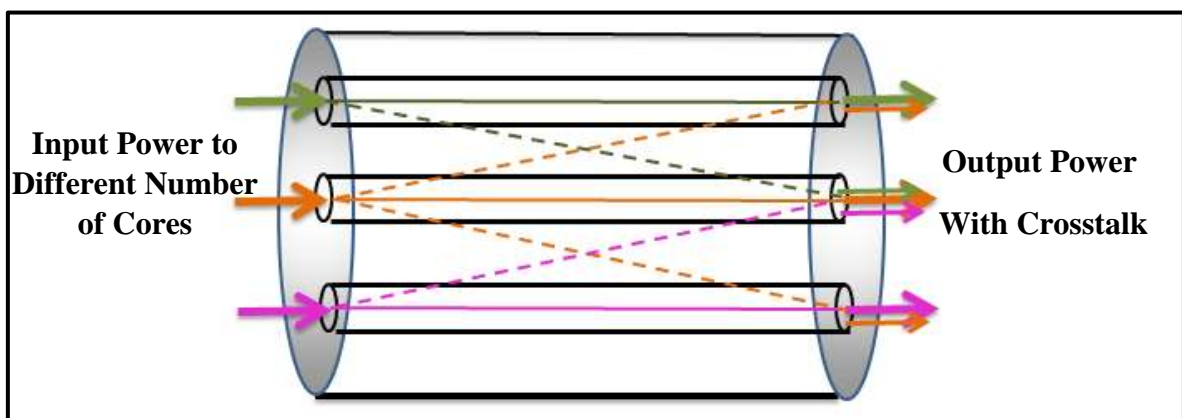


Figure 2-9 Crosstalk between the neighboring cores in MCF.

CHAPTER THREE

Design Issues and Configuration for Tbps MCF-SDM Optical Interconnect

3.1 Introduction

This chapter addresses design issues and configuration for data center optical interconnects (OICs) designed using a hybrid of multicore fiber (MCF)-space division multiplexing (SDM) and wavelength-division multiplexing (WDM) techniques. Each core carries dual polarization (DP) 16-QAM modulation WDM signals. For the purpose of comparison, single-core OICs designed with a single channel or with 16, 24, and 96 WDM channels are investigated here assuming 320 Gbps per channel data rate. Simulation results are obtained using VPIphotonics 9.8 software (see Appendix A).

3.2 Design Concepts for SDM-WDM-DP Interconnect

This section gives design guidelines and brief configuration description of the OIC under investigation. The interconnect uses a multicore fiber; each core supports a single-mode propagation and carries a WDM-DP signal.

3.2.1 Design Guidelines

If the cores transmit identical number of WDM channels N_{ch} and each channel carries the same bit rate R_b , then the total transmitted bit rate R_{bT} through the link is given by

$$R_{bT} = N_c N_{ch} R_b \quad (3.1)$$

where N_c is the number of cores sharing data transmission. If the WDM system in each core operates with Δf channel spacing, then the used optical link bandwidth B_{Link} can be computed by

$$B_{\text{Link}} = N_{\text{ch}} \Delta f \quad (3.2)$$

The spectral efficiency of the link "SE" can be estimated using the following expression

$$\begin{aligned} SE &\equiv R_{\text{bT}}/B_{\text{Link}} \\ &= N_c R_b / \Delta f \end{aligned} \quad (3.3)$$

Note that the spectral efficiency increases linearly with number of cores and it is independent of number of WDM channels N_{ch} in each core.

The symbol rate R_s corresponding to a dual-polarization WDM channel is given by

$$R_s = R_b / 2 \log_2 M \quad (3.4)$$

where M-ary quadrature amplitude modulation (M-QAM) format is assumed for signaling. Note that there is 2 in the denominator of eqn. 3-4 since R_b is the channel bit rate carries by both polarization components. To ensure negligible intersymbol interference (ISI) among the transmitted symbols in each channel, the symbol pulse shape at the input of the receiver decision circuits should have a raised-cosine (RC) spectral profile according to Nyquist criterion. The electrical bandwidth of the transmitted symbol (message) B_{me} depends on the RC roll-off factor r according to [40]

$$B_{\text{me}} = (1 + r) R_s / 2 \quad (3.5)$$

The ideal case of $r = 0$ corresponds to Nyquist filter which has an ideal lowpass spectral characteristics. The other extreme case is when $r = 1$ which gives a full RC spectral shaping and yields a message bandwidth equals R_s .

The optical bandwidth of the message (i.e., the bandwidth of the modulated optical carrier) B_{mo} can be estimated as $2B_{me}$ since the QAM modulator produces a double-sideband signal. To ensure negligible spectral overlapping between successive WDM channels in the same core, the following condition should be satisfied

$$B_{mo} \leq \Delta f \quad (3.6a)$$

This yields

$$R_s \leq \Delta f / (1 + r) \quad (3.6b)$$

The inequality 3.6a is useful for the operation of the optical demultiplexer in the WDM-receiver side so that the required channel can be selected without interfering from adjacent WDM channels.

Two values of channel bit rate R_b are considered in this work, namely 320 and 640 Gbps. The corresponding symbol rates R_s are 40 and 80 Gbps, respectively, when DP 16-QAM signaling is used. The International Telecommunication Union-Telecommunication Sector (ITU-T) has issued different wavelength grids for C-band WDM networks with specific channel spacing Δf , such as 50 and 100 GHz [26]. These values of Δf can be used to implement the two WDM systems considered here, respectively, where the RC roll-factor r is kept below 0.25 (see eqn. 3.6b). Table 3-1 lists the total transmission bit rate R_{bT} as a function of number of cores N_C and number of WDM channels per core. Note that the capacity of the 19-core MCF exceeds 1000 Tbps (= 1 Pbps) when 640 Gbps 96-channel WDM OIC system is used.

In the simulation presented in this thesis, the frequency of the central WDM channel (i.e., the frequency of the unmodulated central laser) is set to 193.1 THz which approximately corresponds to 1550 nm wavelength. The

Table 3-1 Total transmission bit rate for 7- and 19-core MCFs as a function of channel bit rate and number of multiplexed channels.

| Number of Cores | Number of WDM Multiplexed Channels per Core | Total Transmission Bit Rate (Tbps) | |
|-----------------|---------------------------------------------|------------------------------------|------------------|
| | | $R_b = 320$ Gbps | $R_b = 640$ Gbps |
| 7 | 24 | 53.76 | 107.52 |
| | 48 | 107.52 | 215.04 |
| | 72 | 161.28 | 322.56 |
| | 96 | 215.04 | 430.080 |
| 19 | 24 | 145.92 | 291.84 |
| | 48 | 291.84 | 583.68 |
| | 72 | 437.76 | 875.52 |
| | 96 | 583.68 | 1167.36 |

frequencies of other WDM channels spread above and below the central channel frequency by multiple values of Δf . When the number of WDM multiplexed channels N_{ch} is even, the index of the central channel is taken as $1 + (N_{ch}/2)$. This corresponds to 13, 25, 37, and 49 when $N_{ch} = 24, 48, 72,$ and 96. The central channels in different cores are kept under observation during simulation.

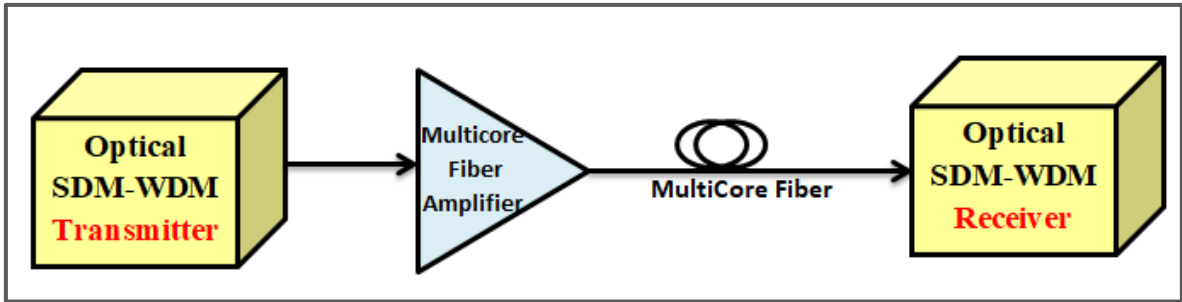
The OICs investigated in this work is based on multicore SDM-WDM-DP configuration and operate with 16-QAM signaling. Each OIC is labelled with three indices, namely $(N_c, N_{ch}, \text{ and } (R_b)_{\text{Gbps}})$ where $(R_b)_{\text{Gbps}}$ denotes the channel bit rate measured in Gbps. For example, the (7, 24, 320) interconnect uses 7-core MCF, 24-channel WDM system per core, and each channel carries 320 Gbps data rate.

3.2.2 System Configuration

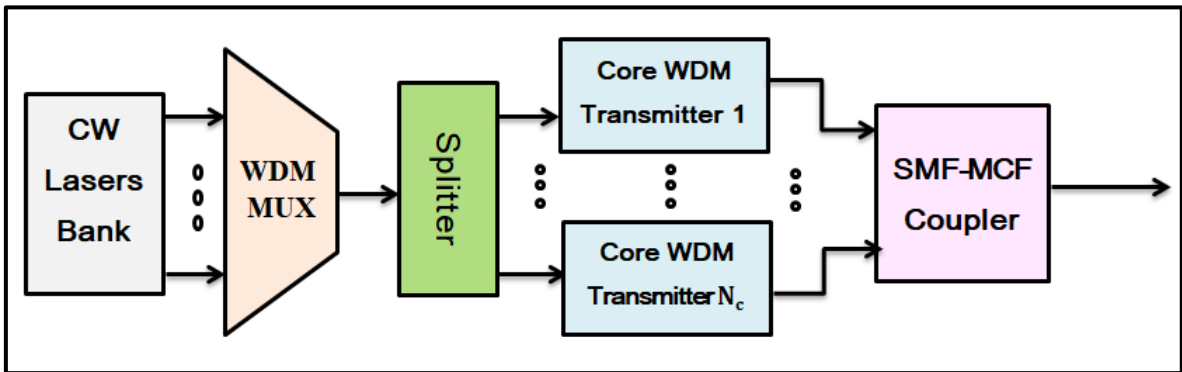
Figure 3-1a shows a simplified schematic diagram of the SDM-WDM OIC while detailed descriptions of the used subsystems are depicted in Figs. 3-1b-d. An MCF amplifier (MCFA) is inserted after the optical SDM-WDM transmitter unit to compensate the transmitter insertion loss and to boost the power of the optical signal launched to the MCF link. For short-length interconnect, no additional optical amplifier is used to compensate the MCF loss.

3.2.2.1 Optical SDM-WDM Transmitter

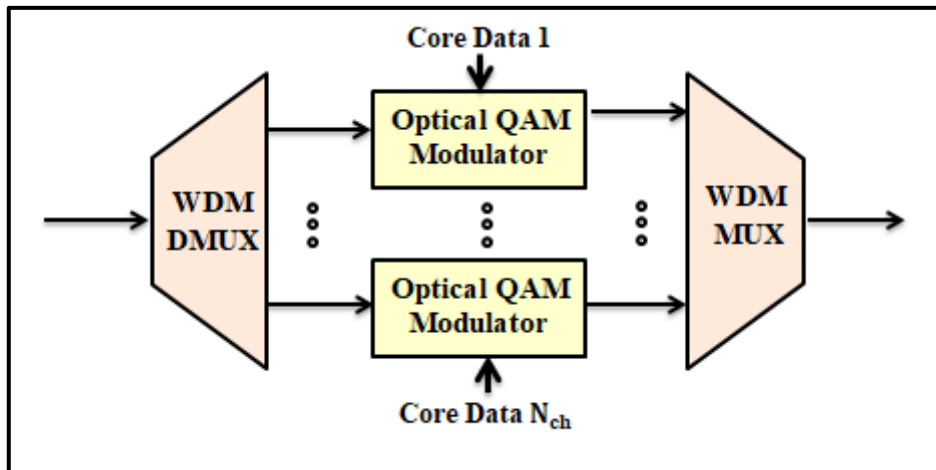
The operation of the SDM-WDM transmitter can be explained with the aid of the block diagram depicted in Fig. 3-1b. Here, a bank of continuous wave (CW) semiconductor lasers is used and these lasers act as a source of unmodulated optical carriers required for each of the core WDM system. The number of these lasers equals the number of WDM channels per core and their frequencies are separated by the channel spacing Δf . The outputs of these CW lasers are combined using a WDM multiplexer to produce an optical waveform containing N_{ch} of equally-spaced unmodulated optical carriers. The resultant waveform is split equally into number of components by using



(a)

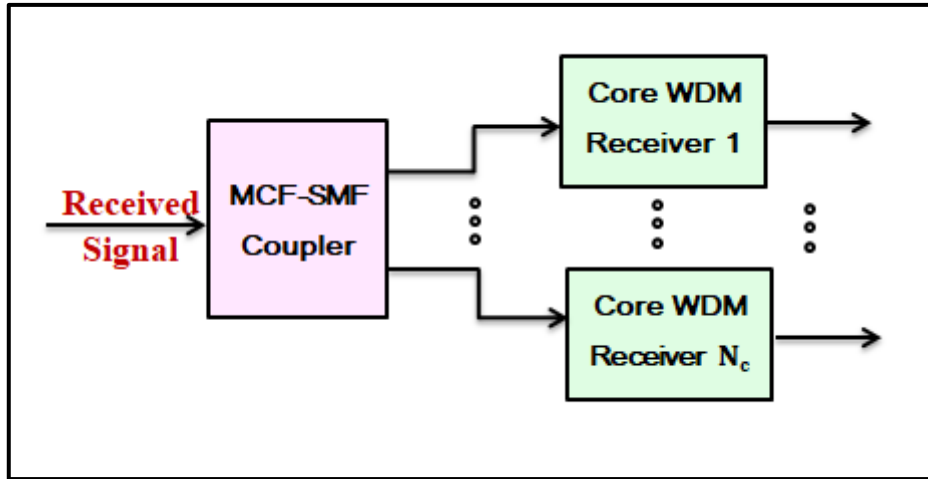


(b)

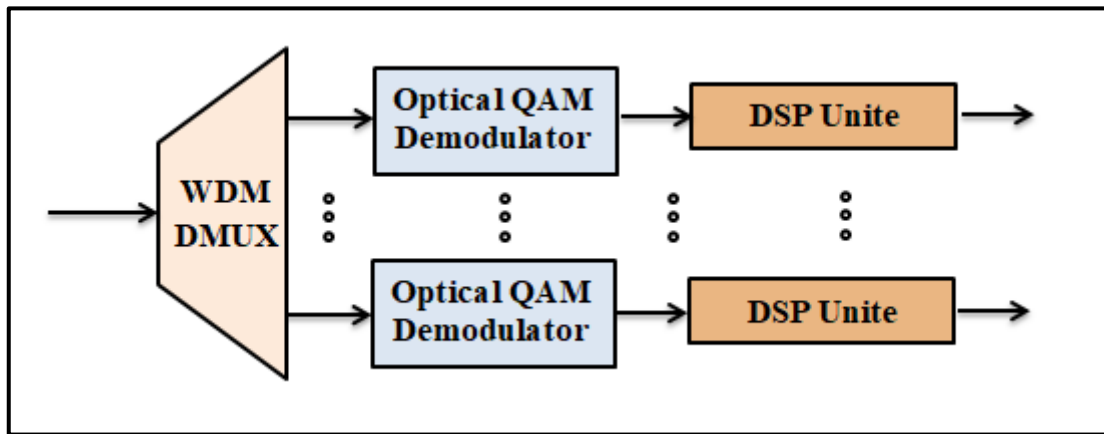


(c)

Figure 3-1 Block diagrams related to SDM-WDM data center interconnect (a) SDM-WDM transmission link (b) SDM-WDM transmitter (c) core WDM transmitter (d) SDM-WDM receiver (e) core WDM receiver.



(d)



(e)

Figure 3-1 (Continued).

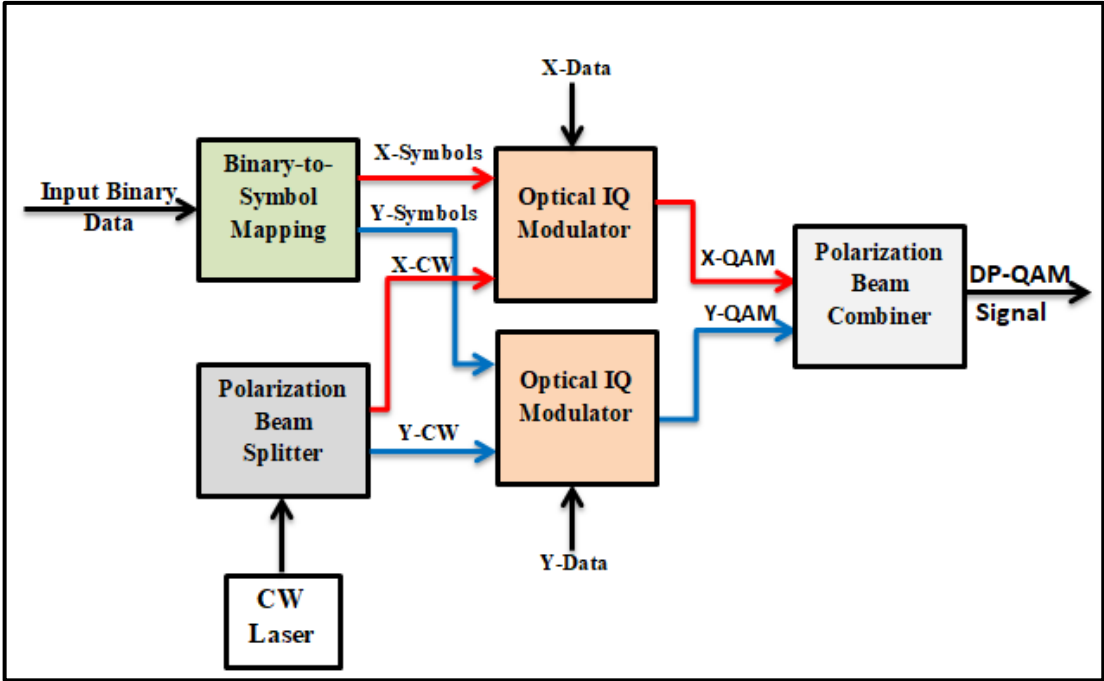
1: N_c optical splitter. Each component acts as unmodulated WDM carriers' source for a specific core. This optical component is then modulated by the data to be transmitted by that core using "core WDM transmitter". The input and output ports of this unit are connected to SMFs. The outputs of the N_c WDM transmitters are coupled to the corresponding N_c cores of the MCF using SMF-MCF coupler.

A simplified block diagram of the core WDM transmitter is illustrated in Fig. 3-1c. The unmodulated WDM carrier's component is split in the frequency domain into N_{ch} unmodulated carriers (i.e., optical carriers) using $1:N_{ch}$ demultiplexer. Each optical carrier is modulated by the corresponding data for that channel of the given core using DP-QAM modulation format. The modulated WDM carriers of each core are multiplexed and the resultant waveform is applied to one of the ports of the SMF-MCF coupler. The generated optical SDM-WDM signal is amplified by the MCFA before launching it to the MCF.

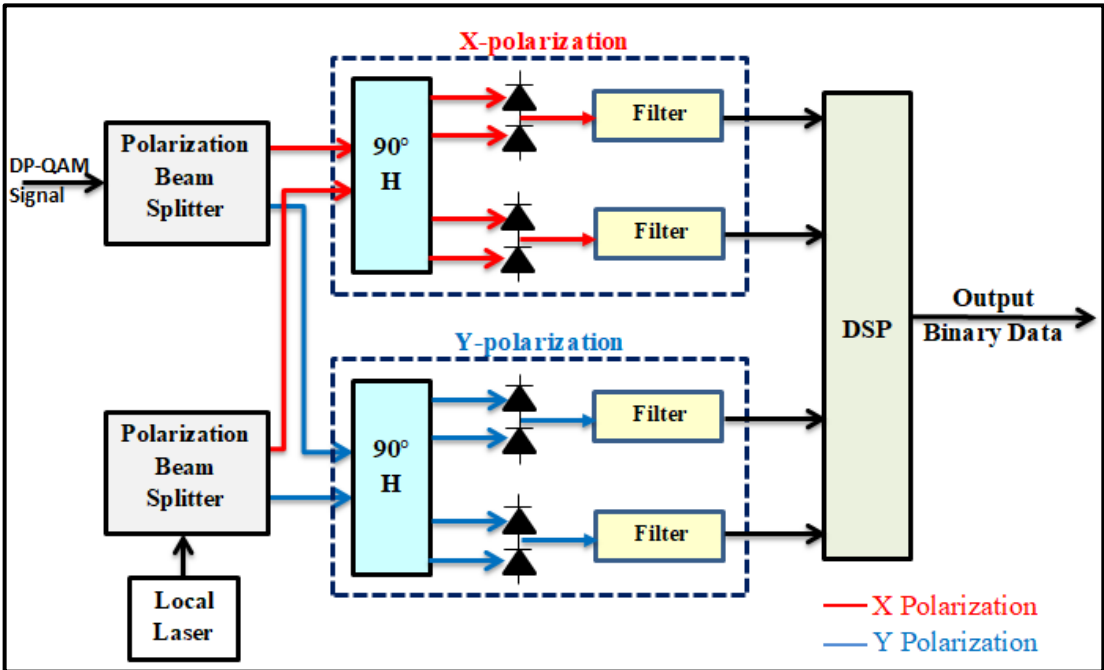
3.2.2.2 Optical SDM-WDM Receiver

The fiber end is connected to the SDM-WDM receiver whose operation is illustrated by the block diagram as shown in Fig. 3-1d. The first stage of this receiver is a MCF-SMF coupler which acts as an interface between the input MCF and N_c output SMFs. Each out port of this coupler is connected to a single-core WDM receiver which uses an $1:N_{ch}$ optical demultiplexer to split the WDM signal received from the coupler output port into N_{ch} components using frequency-domain filtering as shown in Fig. 3-1e. The data is recovered from each demultiplexed channel using digital signal processing (DSP)-based coherent DP-QAM demodulator.

The optical DP-QAM transmitter and receiver for each one of the WDM channels are designed according to the block diagrams shown in Figs. 3-2a and b, respectively. The transmitter generates an optical polarization multiplexed signal (i.e., DP modulated signal) using a pair of in-phase quadrature-phase (IQ) modulators to independently modulate each of the polarization component of the optical carrier wave. The transmitter uses a linearly polarized CW laser with 45° polarization angle to ensure equal power



(a)



(b)

Figure 3-2 Block diagrams of optical DP-QAM system(a) transmitter (b) receiver.

in the two orthogonal polarization components. A polarization beam splitter (PBS) splits the laser optical output into two equal-power and orthogonally polarized CW components (X-and Y-polarizations). These two components are applied to two identical QAM modulators used for the X-polarized and Y-polarized channels. The binary data are applied to a binary-to-symbols mapper which produces two groups of symbols (X-symbols and Y-symbols). Each one of the symbol groups is used to derive one of the two QAM modulators and therefor modulates the corresponding optical carrier polarization component. The two generated modulated signals X-QAM and Y-QAM are then combined using polarization beam combiner (PBC) to produce the DP signaling format.

The DP-QAM receiver is a polarization diversity digital coherent receiver and its operation is based on optical coherent quadrature receiver model. The receiver uses a 45° linearly polarization CW local laser which acts as a local oscillator (LO) and whose frequency should match the frequency of the transmitter unmodulated optical carrier of that channel. For each one of the WDM channels, the corresponding received (demultiplexed) optical modulated carrier and the output of the channel LO are splitted into two orthogonal polarized components using two separated PBSs. Two 90° optical hybrids are used to combine the received signal and the LO field component, in each polarization state. This 90° hybrid device acts as a 2×4 quadrature optical hybrid. It combines two input signals (LO reference signal and received signal) and generates four output optical signals with 90° phase shift. The ideal transmission matrix of this hybrid is governed by [41]

$$\begin{bmatrix} E_{01} \\ E_{02} \\ E_{03} \\ E_{04} \end{bmatrix} = \frac{1}{2} \begin{bmatrix} 1 & 1 \\ 1 & -1 \\ 1 & j \\ 1 & -j \end{bmatrix} \begin{bmatrix} E_{i1} \\ E_{i2} \end{bmatrix} \quad (3.7)$$

where E_{ik} and E_{ok} denote the electric fields at the input and output ports of the device, respectively. The first two outputs, E_{01} and E_{02} are applied to a balanced photoreceiver (BPR) to generate the in-phase (I) component of the detected symbol. The next two outputs E_{03} and E_{04} are applied to another BPR to generate the quadrature-phase (Q) component of the detected symbol.

The BPR uses two identical photodiodes (PDs) to extract the mixing component between the applied fields of the received signal and reference signal (i.e., LO field). To illustrate this operation, let $E_{i1} = a_s + jb_s$ represents the received symbol where a_s and b_s denote the amplitudes of the cosine (I) and sine (Q) components of the carrier, respectively. Let $E_{i2} = a_{LO}$ represents the amplitude of the local oscillator field $e_{LO}(t) = a_{LO} \cos \omega_c t$. According to eqn. 3.7

$$E_{01} = (a_s + a_{LO}) + jb_s \quad (3.8a)$$

$$E_{02} = (a_s - a_{LO}) + jb_s \quad (3.8b)$$

The PD generates a photocurrent I_{PD} proportional to the absolute value of the incident field. Therefore, the two balanced PDs generate the following pair of photocurrents

$$\begin{aligned} I_{PD1} &= \mathcal{R}|E_{01}|^2 \\ &= \mathcal{R}[a_s^2 + 2a_s a_{LO} + a_{LO}^2 + b_s^2] \end{aligned} \quad (3.9a)$$

$$\begin{aligned} I_{PD2} &= \mathcal{R}|E_{02}|^2 \\ &= \mathcal{R}[a_s^2 - 2a_s a_{LO} + a_{LO}^2 + b_s^2] \end{aligned} \quad (3.9b)$$

where \mathcal{R} is the PD responsivity measured in A/W. The net photocurrent generated by the BPR is given by

$$I_I \equiv I_{BPR1} = I_{PD1} - I_{PD2} = 4\mathcal{R}a_{LO}a_s \quad (3.10a)$$

In a similar way, one can show that the second BPR generates the following net photocurrent as a response for the applied fields E_{03} and E_{04}

$$I_Q \equiv I_{BPR2} = I_{PD3} - I_{PD4} = 4\mathcal{R}a_{LO}b_s \quad (3.10b)$$

Note that the photocurrents I_{BPR1} and I_{BPR2} are proportional to the I and Q amplitudes of the received symbol, respectively, and the proportionality constant depends linearly on the amplitude of the LO field.

The DP receiver uses four BPRs; two for each polarization to produce the photocurrents I_{IX} (I_{IY}) and I_{QX} (I_{QY}). Each of these four current waveforms is then applied to a lowpass and shaping filter followed by an analogue-to-digital convertor (ADC). The four digital currents are applied to a dual-polarization digital signal processing (DSP) unit. This unit is used to perform various DSP steps required in coherent single-carrier communication systems utilizing single-polarization or dual-polarization modulation formats. The unit is provided with a range of DSP algorithms to perform different procedures. Among these procedures, which are used in this works are

- (i) Compensation of chromatic dispersion (CD) and polarization-mode dispersion (PMD) of the fiber.
- (ii) Carrier frequency recovery (CFR) and carrier phase recovery (CPF).
- (iii) Matched-filter equalization.
- (iv) An adaptive multi-input multi-output (MIMO) time-domain equalizer (TDE).

3.3 Performance of a Single-Core Optical Interconnect

This section presents simulation results describing the transmission performance of a single-core OIC supporting single or WDM channel transmission. Results related to multicore fiber link will be addressed in details in chapter four. The core carries 320 Gbps DP 16-QAM signal per channel. Unless otherwise stated, the main parameters values used in the simulation are given in Table 3-2.

The transmission link under observation consists of multi 100 km-loss compensated span. Each span has 100 km-length single-core fiber cascaded with 20 dB optical amplifier (OA) to compensate the fiber loss. A booster OA is inserted after the optical transmitter to compensate partially or completely the optical modulator insertion loss and to enhance the level of the optical power launched to the fiber.

The investigation starts by considering the special case where the single-core fiber carries a single channel. Figures 3-3a-d depict the dependence of the receiver BER as a function of transmitter laser power P_{LT} for 2-, 3-, 4-, and 5-span OICs, respectively. The gain of the booster OA is set to 17.2 dB to compensate the optical transmitter insertion loss. Investigating the results in Fig. 3.3 reveals the following findings

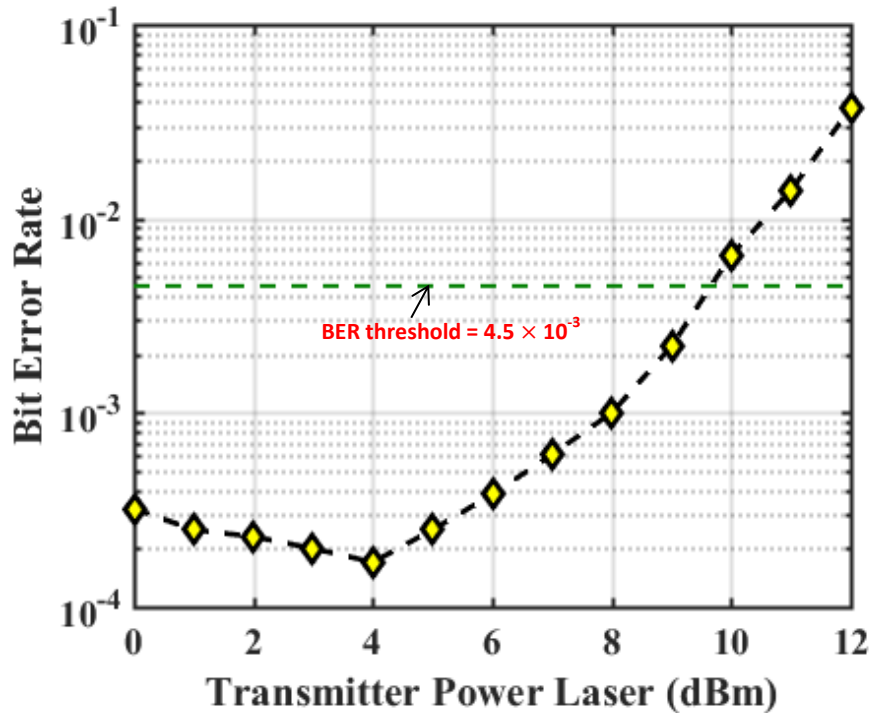
- i. Due to the fiber nonlinear optics, there is an optimum value of transmitter laser power, $(P_{LT})_{opt}$ which minimizes the BER. The values of $(P_{LT})_{opt}$ are 4, 3, 4, and 2 dB when number of spans $N_{span} = 2, 3, 4, \text{ and } 5$, respectively. The corresponding BER = 1.7×10^{-4} , 6.4×10^{-4} , 2.2×10^{-3} , and 4.6×10^{-3} , respectively.

Table 3-2 Parameters values used in the simulation.

| Subsystem | Component | Parameter | Value | Remark |
|---------------------|------------------------------------|----------------------------------------|--------------------------------------------|------------------------------------------------------------|
| SDM-WDM Transmitter | Lasers Bank | laser power | 5mW | |
| | | Central frequency | 193.1 THz | |
| | | Channel spacing | 50 and 100 GHz | |
| | | Linewidth | 100 kHz | |
| | Optical Modulation | Modulation format | DP 16-QAM | Optical IQ modulation based on Mach-Zehnder configuration. |
| | | V_{π} | 5 V | |
| | | Insertion loss | 6 dB | |
| | | Extinction ratio | 35 dB | |
| | Optical Multiplexer /Demultiplexer | Insertion loss | 5 dB (each) | Based on arrayed waveguide grating |
| | SMF-Multicore Coupler | Insertion loss | 0 | Ideal |
| Coupling efficiency | | 100% | | |
| Transmission Link | Multicore Fiber Amplifier | Gain | 17.2 dB | Gain controlled mode of operation |
| | | Noise figure | 4 dB | |
| | | Number of cores | 7 and 19 | |
| | | Polarization dependence | Neglected | |
| | Multicore Fiber | Number of cores | 7 and 19 | |
| | | Length | 10 km | |
| | | Number of modes | Single mode | |
| | | Loss at 193.1 THz | 0.2 dB/km | |
| | | Group velocity dispersion at 193.1 THz | 17 ps/(nm.km) | |
| | | Dispersion slope at 193.1 THz | 0.075 ps/(nm ² .km) | |
| | | Nonlinear index | $2.6 \times 10^{-20} \text{ m}^2/\text{W}$ | |
| | | Core effective area | $80 \mu\text{m}^2$ | |
| | Multicore-SMF Coupler | Insertion loss | 0 | Ideal |
| | | Coupler efficiency | 100% | |
| SDM-WDM Receiver | Local Lasers Bank | Laser power | 5 mW | |
| | | Central frequency | 193.1 THz | |
| | | Channel spacing | 50 and 100 GHz | |
| | | Linewidth | 100 kHz | |
| | 90° Hybrid | Insertion loss | 0 dB | Ideal |
| | Photodiode | Responsivity | 1 A/W | |
| | | Dark current | 0 | |
| | Lowpass Filter | Order | 4 | |
| Bandwidth | | Baud rate | | |

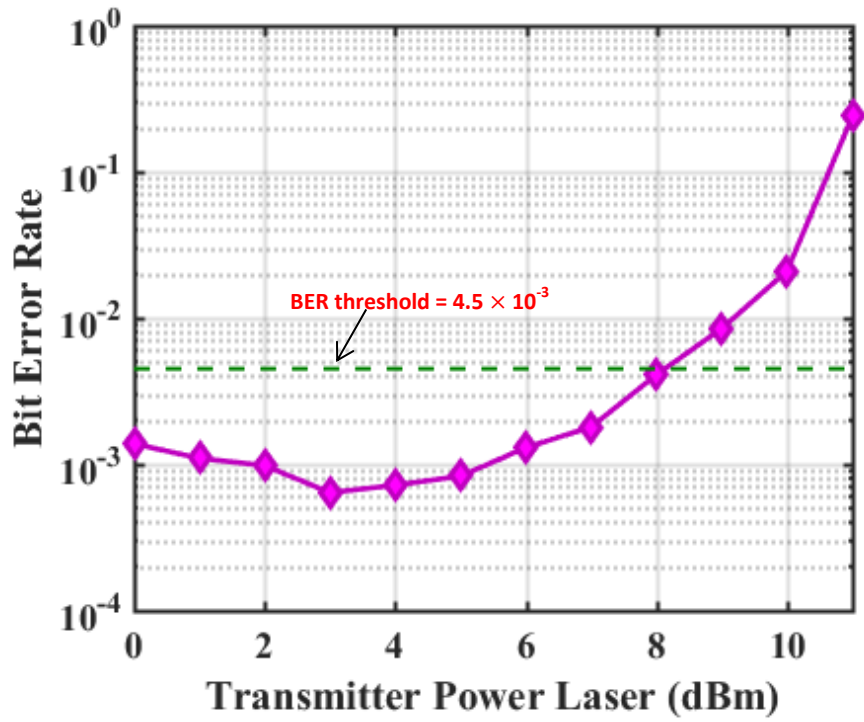
- ii. Assuming threshold BER, BER_{th} , of 4.5×10^{-3} which corresponds to 7% hard-decision (HD) forward error correcting (FEC) code [42], then the 5-span OIC cannot give satisfactory transmission performance when $P_{LT} = 0$ dBm. In contrast, using N_{span} less than 5 can support satisfactory transmission when $P_{LT} = 0$ dBm.

The next step is to assess the effect of booster amplifier gain G_b on the transmission performance of the single-core single-channel OIC. Figure 3-4 displays the relation between BER and the length of the transmission link L when $P_{LT} = 5$ mW (7 dBm) and assuming no booster amplifier is used. The maximum transmission reach L_{max} , which yields $BER = BER_{th}$, is estimated to be 195 km.

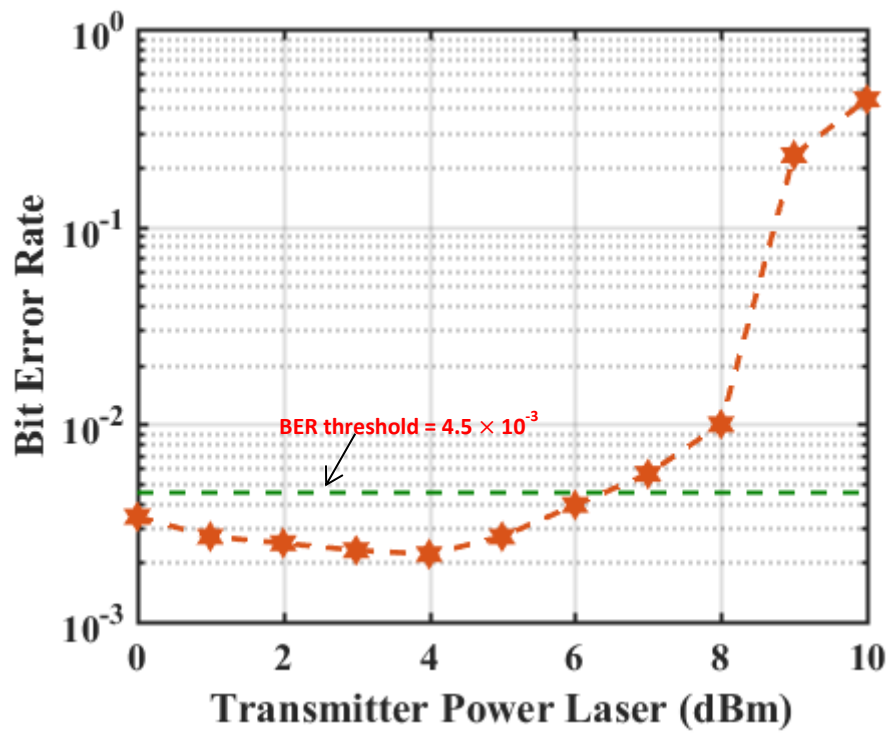


(a)

Figure 3-3 BER versus power laser transmitter for a single-core fiber carrying a single channel for different number of link spans (a) $N_{span}=2$ (b) $N_{span}=3$ (c) $N_{span}=4$ (d) $N_{span}=5$.

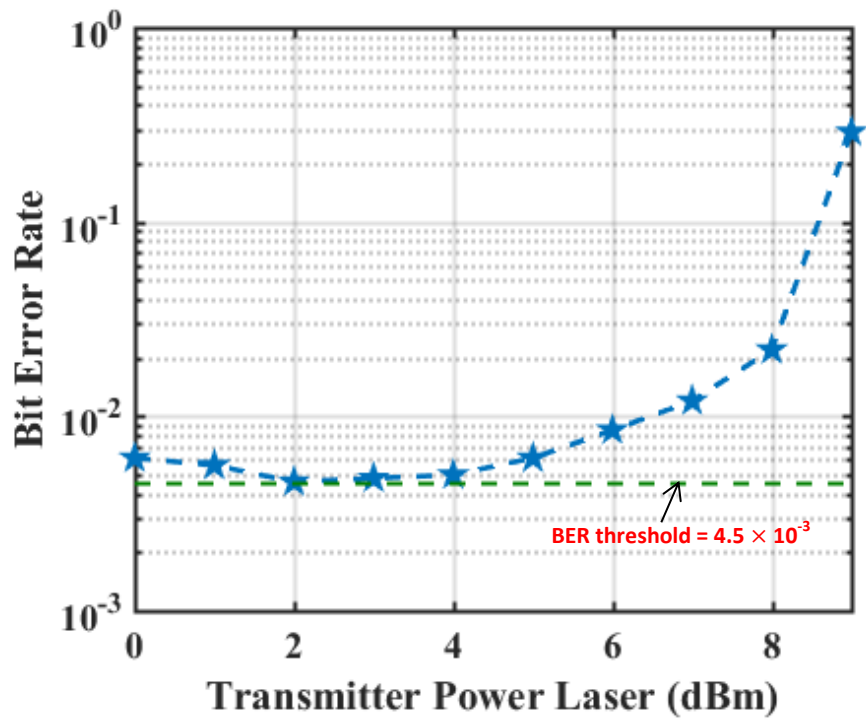


(b)



(c)

Figure 3-3 (Continued).



(d)

Figure 3-3 (Continued).

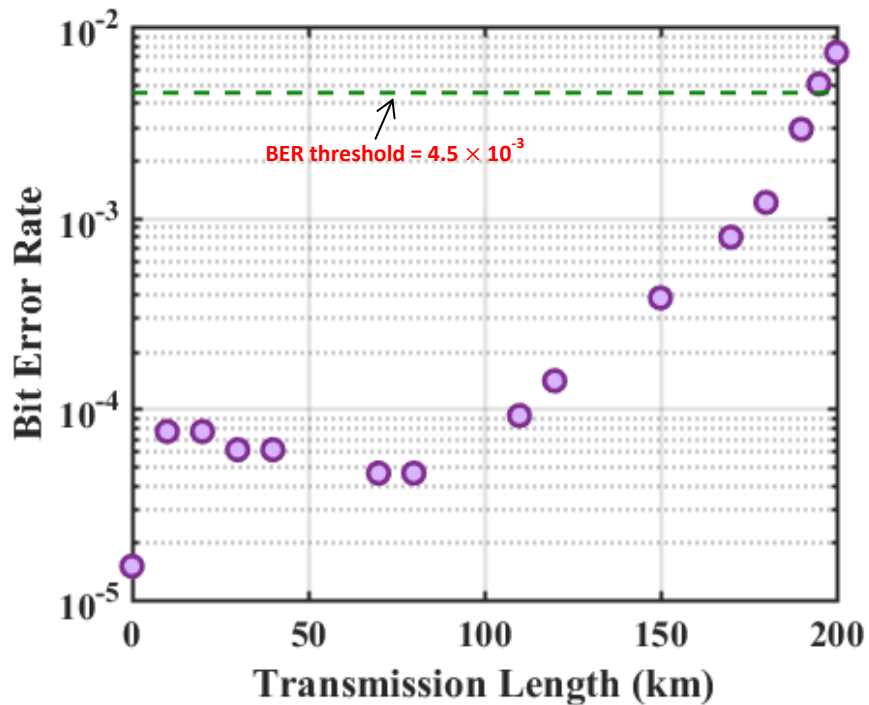


Figure 3-4 Variation of BER with transmission length for 320 Gbps DP 16-QAM single-core single-channel OIC operating in the absence of booster amplifier.

Figure 3-5 illustrates the dependence of L_{\max} on P_{LT} in the absence of booster amplifier. Note that increasing P_{LT} from 0 to 10 dBm will increase the transmission reach by 45 km. This is to be compared with $\Delta P_{LT}/\alpha = 10/0.2 = 50$ km, where $\alpha = 0.2$ dB/km is the loss coefficient of the fiber at 1550 nm wavelength. This indicates that the OIC operates without nonlinear fiber effect when designed to transmit one channel in the absence of booster amplifier.

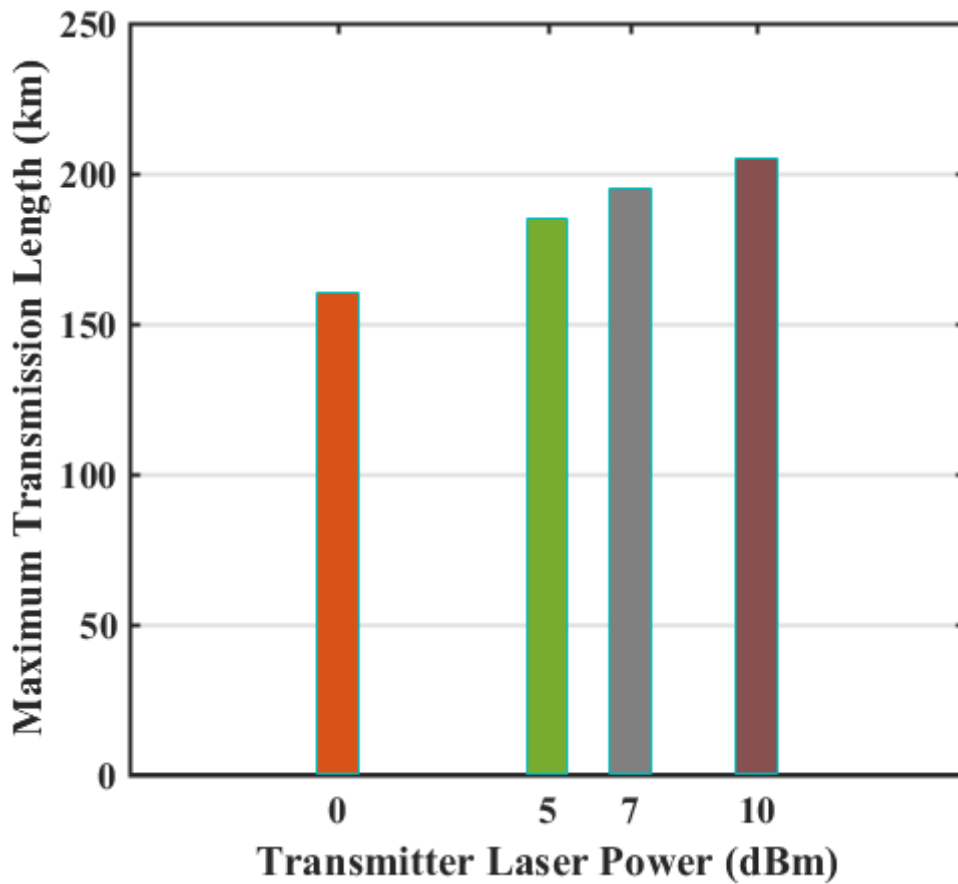
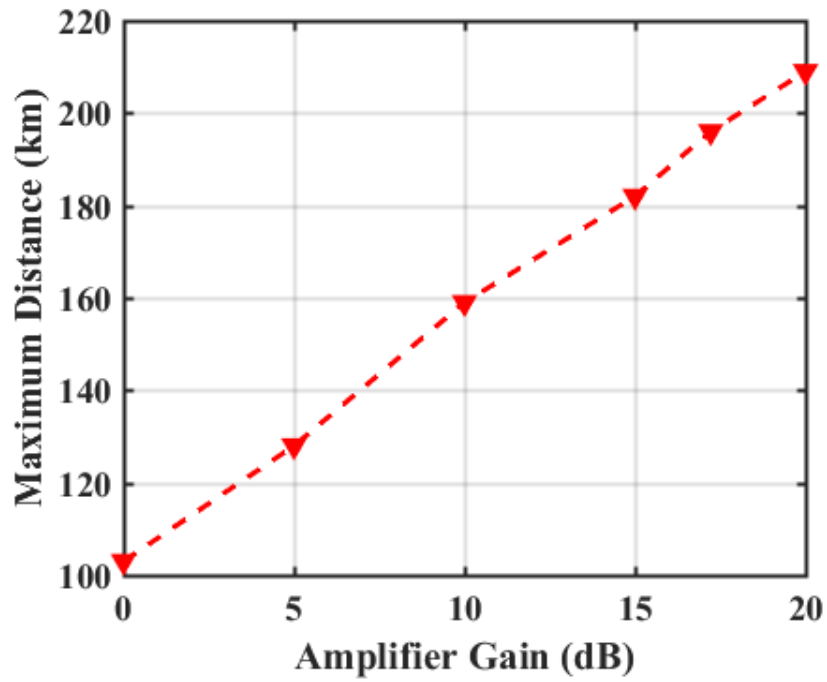
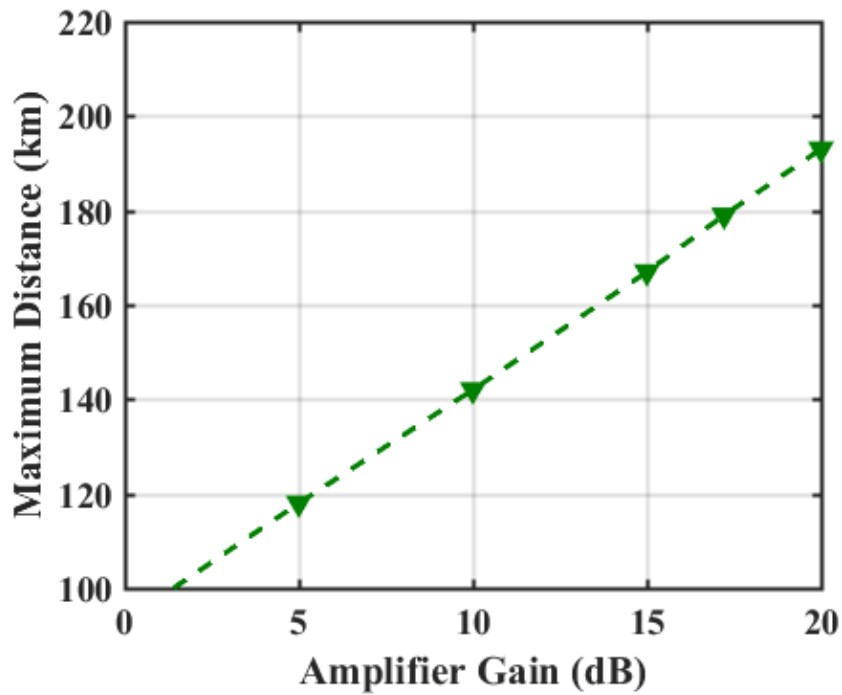


Figure 3-5 Maximum reach versus transmitter power laser for 320 Gbps DP 16-QAM single-core single-channel OIC operating without booster amplifier.

The simulation is carried further to investigate the performance of a single-core WDM interconnect. Figures 3-6a-c display the maximum reach

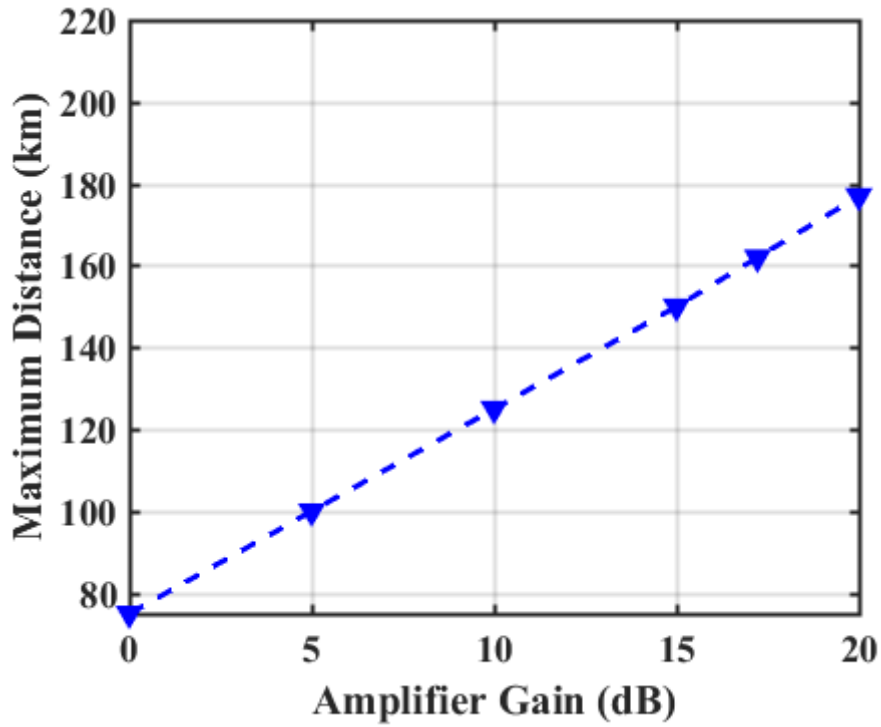


(a)



(b)

Figure 3-6 Effect of number of WDM multiplexed channels on maximum reach for 320 Gbps DP 16-QAM single-core single-channel OIC. (a) 16-channel (b) 24-channel (c) 96-channel



(c)

Figure 3-6 (Continued).

L_{\max} for different values of booster amplifier gain and assuming the number of WDM multiplexed channels N_{ch} is equal to 16, 24, and 96, respectively. In this simulation, $P_{\text{LT}} = 5$ mW, the central channel laser frequency = 193.1 THz, and channel spacing = 50 GHz. Note that L_{\max} increases with booster amplifier gain for all the three values of N_{ch} . An addition, note further as N_{ch} increases, L_{\max} decreases for the same value of P_{LT} . This comes from the effect of fiber nonlinearity.

3.4 Calculation of Intercore Crosstalk

This section presents the simplified mathematical framework supported by numerical values for MCF intercore crosstalk and based on eqns. 3.11 and

3.12 which describe the power leakage from core to core in MCF can be expressed as [14, 39]

$$h = \frac{2k^2 R}{\beta C_p} \quad (3.11)$$

where

h = Power leakage (m^{-1})

k = Coupling coefficient (m^{-1})

R = Bending radius (m)

β = Propagation constant (m^{-1})

C_p = Core pitch (m)

In the unidirectional transmission, a homogeneous MCF's crosstalk level can be calculated using eqn. 3.12 [14, 39]

$$CT = \frac{n_a(1-e^{-2hL(n_a+1)})}{1+n_a e^{-2hL(n_a+1)}} \quad (3.12)$$

where

CT = Intercore crosstalk

n_a = Number of adjacent cores

L = Fiber length

In decibel measure, CT (dB) = 10 Log CT . From eqn. 3.13a, one can see that the value of L corresponds to certain CT level is given by

$$L_{CT} = \frac{1}{2(n_a+1)h} \ln \frac{n_a(1+CT)}{n_a-CT} \quad (3.13a)$$

Note that $CT=1W$ (i.e., 0dB) occurs when $L \equiv L_{0dB}$

$$L_{0dB} = \frac{1}{2(n_a+1)h} \ln \frac{2n_a}{n_a-1} \quad (3.13b)$$

Now consider the following two limiting cases corresponding to $L \gg L_{critical}$ or $L \ll L_{critical}$ where the critical length is given by

$$L_{critical} = 1/[2(n_a + 1)h] \quad (3.13c)$$

Case I: $L \gg L_{critical}$

In this case, $e^{-2hL(n_a+1)}$ approaches zero and this leads to

$$CT = n_a \quad (3.14)$$

(i.e., $CT > 0dB$).

Case II: $L \ll L_{critical}$

In this case, $e^{-2hL(n_a+1)} \approx 1 - 2hL[(n_a + 1)]$. Then eqn. 3.12 reduces to

$$CT \approx 2n_a(n_a + 1)hL \quad L \ll L_{critical} \quad (3.15)$$

Equation 3.15 reveals that the crosstalk increases linearly with L and has n_a^2 dependence.

Table 3-3 lists the calculated values of L_{0dB} and $L_{critical}$ corresponding to four types of homogenous MCF designed with different core pitch C_p and bending radius R . The values of coupling coefficients k are taken from Ref. [32] and the propagation constant β is calculated from $\beta = 2\pi n/\lambda$ where n is the core refractive index. At $\lambda=1550$ nm, $n \approx 1.45$ which gives $\beta = 5.9 \times 10^6 \text{ m}^{-1}$.

It is worth to mention here that the coupling coefficient is strongly dependent on the core pitch. Going from $C_p = 40 \mu\text{m}$ to 35 and 30 μm will

Table 3-3 L_{0dB} and $L_{critical}$ values correspond to four homogeneous MCF forms, constructed with different C_p and R .

| Fiber Type | Fiber Parameter | | | Calculated Parameters | | |
|----------------|-----------------|----------------------|---------|-----------------------|--------------------|--------------------|
| | $C_p(\mu m)$ | $k(m^{-1})$ | $R(mm)$ | $h(m^{-1})$ | $L_{0dB}(km)$ | $L_{critical}(km)$ |
| Fiber 1 | 40 | 4×10^{-4} | 50 | 6.8×10^{-11} | 9.2×10^5 | 1.05×10^6 |
| Fiber 2 | 35 | 3.5×10^{-3} | 50 | 5.9×10^{-9} | 1.06×10^4 | 1.2×10^4 |
| Fiber 3 | 30 | 6×10^{-2} | 50 | 2.0×10^{-6} | 31.3 | 35.7 |
| Fiber 4 | 30 | 6×10^{-2} | 10 | 4×10^{-7} | 156.3 | 178.5 |

increases k by 8.75 and 150 time, respectively. Note also that the parameter h has k^2 dependence and $L_{critical}$ is inversely proportional to h . Thus, it is expected that $L_{critical}$ will be reduced approximately by $(8.75)^2 = 76.6$ and $(150)^2 = 22500$ when C_p is changed for 40 μm to 35 and 30 μm , respectively.

Using eqns. 3.13a and c yields the follow relation between the two fiber lengths L_{CT} and $L_{critical}$.

$$L_{CT} = \left[\ln \frac{n_a(1+CT)}{n_a-CT} \right] L_{critical} \quad (3.16)$$

Table 3-4 lists the calculated values of L_{CT} of the four fiber types corresponding to different crosstalk levels. It is cleared from Table 3-3 that fiber 2 is suitable for designing short-and medium, reach OICs with negligible crosstalk ($< -20\text{dB}$).

Table 3-4 Fiber lengths corresponding to various crosstalk levels.

| Fiber Type | $L_{CT}(km)$ | | |
|------------|----------------------|----------------------|----------------------|
| | $CT = -20\text{ dB}$ | $CT = -15\text{ dB}$ | $CT = -10\text{ dB}$ |
| Fiber 1 | 1.2×10^4 | 3.5×10^4 | 1.2×10^5 |
| Fiber 2 | 136.6 | 433.2 | 1320 |
| Fiber 3 | 0.4 | 1.3 | 3.9 |
| Fiber 4 | 2 | 6.4 | 19.6 |

CHAPTER FOUR

Simulation Results for MCF-Based SDM Optical Interconnect

4.1 Introduction

The effect of intercore crosstalk on the transmission performance of optical interconnect (OIC) is investigated in this chapter under various link parameters, namely number of cores N_c , number of WDM channels per core N_{ch} , bit rate per channel R_b , and fiber length L . Simulation results are reported for $R_b = 320$ and 640 Gbps, $N_c = 7$ and 19 , N_{ch} up to 96 , and assuming DP 16-QAM modulation format. The effect of fiber nonlinearity on the transmission performance of medium and long-reach OIC designed with MCF-based SDM-WDM configuration is also presented in Section 4.4. The simulation is performed using VPIphotonics 9.8 software.

4.2 Simulation of (7, 24, 320) Interconnect

This section presents simulation results related to a 7-core interconnect with each core supports a single-mode operation. Each core carries 24 channel C-band WDM subsystem and each channel operates with 320 Gbps DP 16-QAM signaling. Few remarks related to the simulated system are presented in Section 4.2.1.

4.2.1 Remarks Related to the Simulated System

- (i) The symbol rate for each WDM channel is $R_s = 40$ GSps ($= 320$ Gbps/ (2×4)). Therefore, WDM channel spacing Δf of 50 GHz is used in the simulation. The thirteenth channel (Ch13) is taken as the central channel where the corresponding unmodulated laser operates at

193.1 THz frequency. The frequencies of other transmitter WDM lasers span from 192.5–193.65 THz with 50 GHz channel spacing.

- (ii) The total bit rate R_{bT} carries by the SDM interconnect equals $N_C N_{ch} R_b = 7 \times 24 \times 320 \text{ Gbps} = 53.76 \text{ Tbps}$. Here N_C , N_{ch} and R_b stand for the number of cores, number of WDM channels per core, and bit rate of each WDM channel, respectively.
- (iii) The spectral efficiency SE of the interconnect is given by $N_C N_{ch} R_b / N_{ch} \Delta f = N_C R_b / \Delta f = 44.8 \text{ b/Hz}$. Note that the total optical transmission bandwidth ($= N_{ch} \Delta f$) = 1.2 THz.

The primary simulation results reveal that when the power of each unmodulated transmitter laser P_{LT} is set to 5 mW (= 7 dBm), the SDM transmitter offers a total output power of 3.5 dBm. Thus, the insertion loss of this transmitter equals $10 \log(24 \times 5) - 3.5 = 17.3 \text{ dB}$. Therefore, an optical amplifier (OA) may be inserted after the SDM transmitter to act as a booster amplifier to enhance the power launched to the MCF. When a 17.3 dB-booster amplifier is used, the insertion loss of the SDM transmitter is completely compensated.

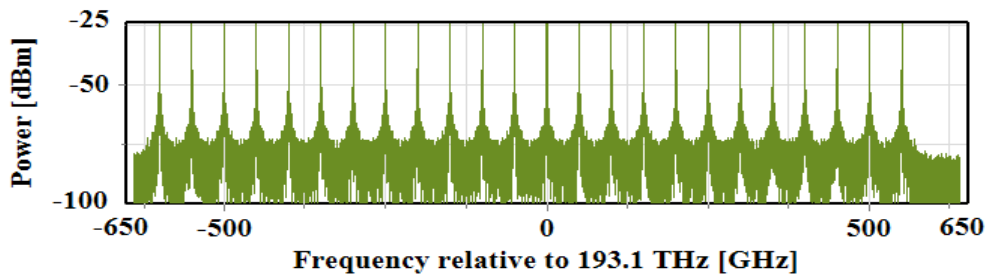
The performance of the OIC under investigation is estimated under the assumption that the maximum acceptable bit error rate (BER), i.e. threshold BER “BER_{th}”, is 4.5×10^{-3} . This corresponds to 7% hard decision (HD) forward error correcting (FEC) code.

4.2.2 Transmission Performance of (7, 24, 320) OIC

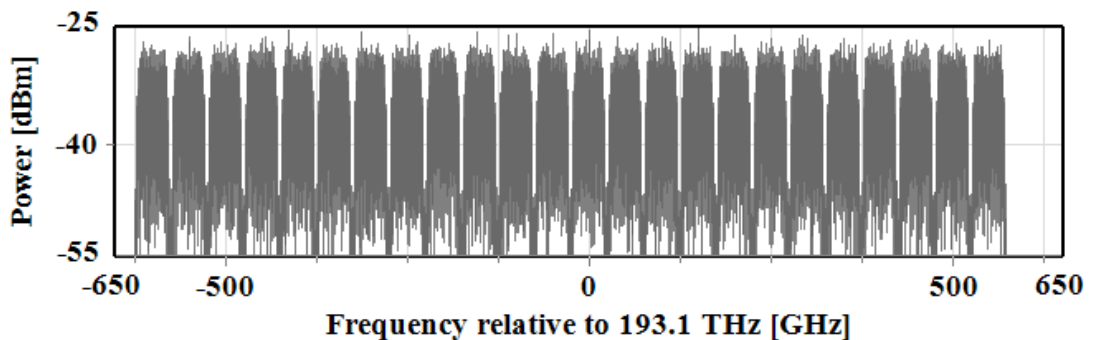
This subsection addresses the transmission performance of the (7, 24, 320) OIC operating in the presence of intercore crosstalk. The first point of investigation is related to an interconnect of length $L=10 \text{ km}$ and uses

5 mw-lasers (i.e., $P_{LT} = 7\text{dBm}$) and a booster OA of gain $G_b = 17.3\text{ dB}$. The central channel Ch13 is kept under observation during the investigation. The results reveal that almost error less transmission is achieved when the crosstalk level CT is below -25 dB .

Figure 4-1 illustrates the optical spectra of the signals at different points of the system when the interconnect operates with -20 dB crosstalk. The figure also contains constellation diagrams corresponding to Ch13 received in three different cores (core1, core5, and core7) where an average receiver BER of 1.0×10^{-3} is reported.

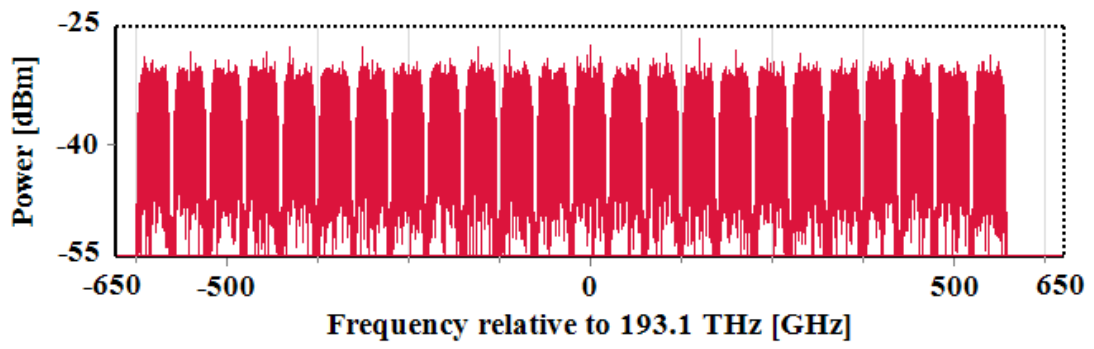


(a)

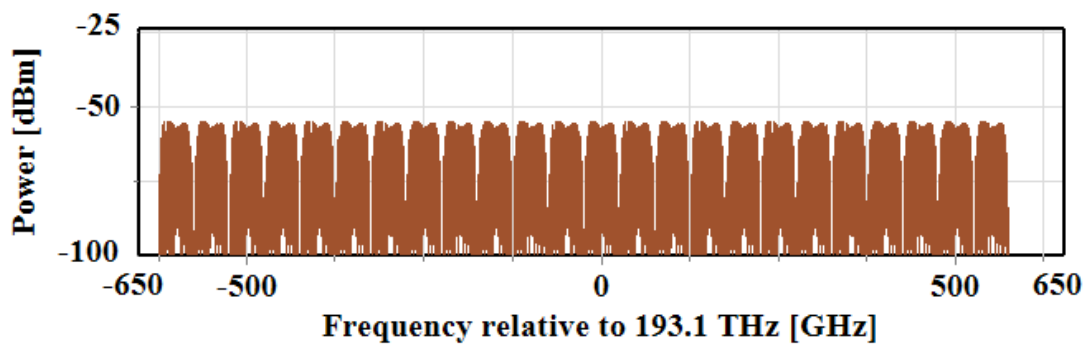


(b)

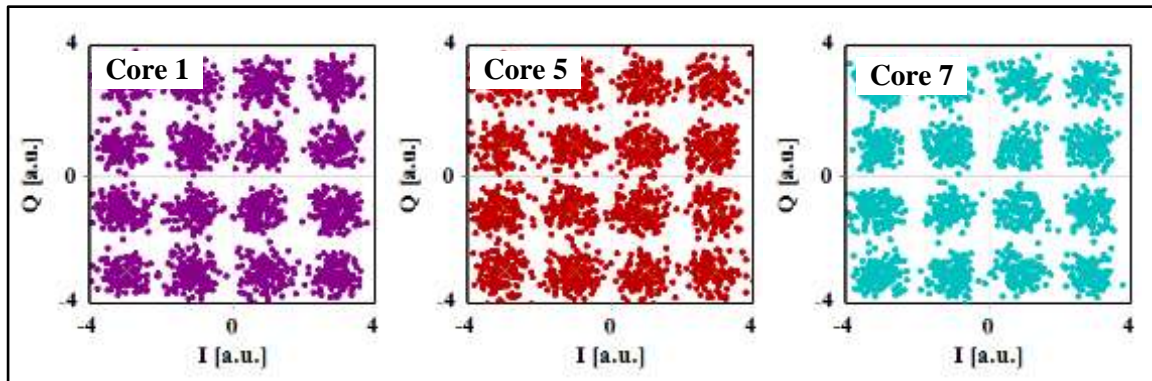
Figure 4-1 Optical spectra and constellation diagrams related to (7, 24, 320) OIC operating with -20 dB crosstalk (a) unmodulated WDM optical carriers (b) amplified SDM-WDM transmitter signal (c) optical signal after 10 km transmission (d) intercore crosstalk signal (e) constellation diagrams corresponding to Ch13 received in three different cores (core1, core5, and core7).



(c)



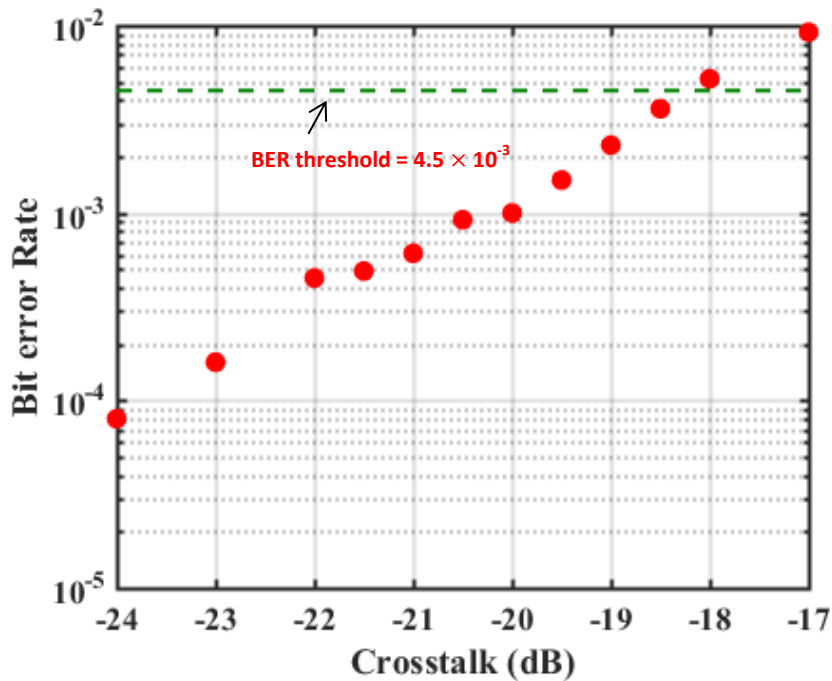
(d)



(e)

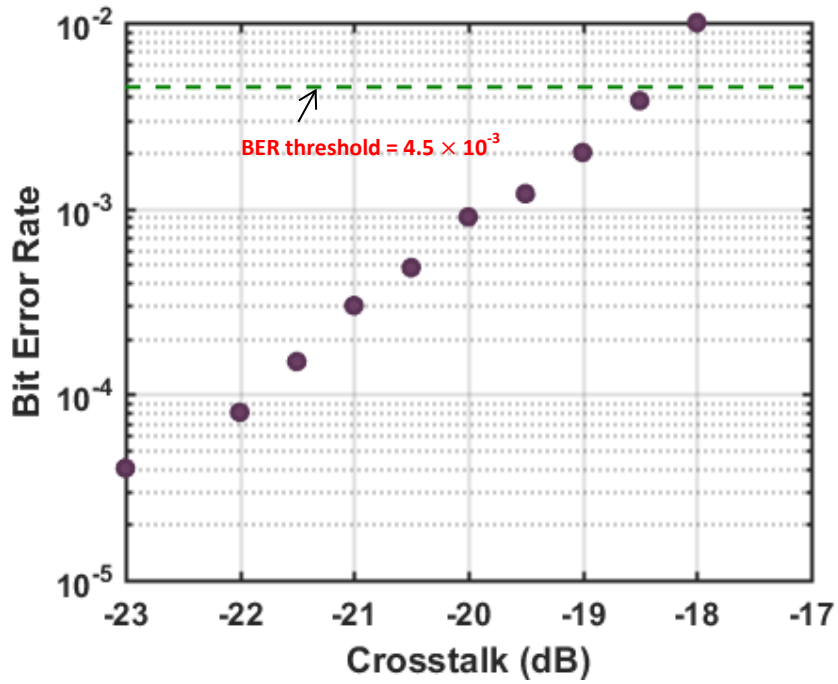
Figure 4-1 (Continued).

The variation of BER with crosstalk level is displayed in Figs. 4-2a and b for 10 km- and 20 km-OIC, respectively. Investigating the results reveals that a BER less than the threshold ($BER_{th} = 4.5 \times 10^{-3}$) is achieved when CT is less than -18.5 dB for both OICs. Table 4-1 lists the dependence of BER on transmitter laser power P_{LT} when the 10 km-link operates with either -20 dB crosstalk or without crosstalk. Note the threshold BER can be achieved with $P_{LT} = 2$ mW when -20 dB crosstalk exists. This is to be compared with $P_{LT} = 1$ mW in the absence of crosstalk.



(a)

Figure 4-2 Variation of BER with intercore crosstalk for (7, 24, 320) OIC after transmission length of (a) 10 km (b) 20 km.



(b)

Figure 4-2 (Continued).

Table 4-1 Effect of transmitter laser power on BER for (7, 24,320) 10 km interconnect.

| Transmitter Laser Power (mW) | Bit Error Rate | |
|------------------------------|----------------------|-----------------------|
| | Without Crosstalk | With -20 dB Crosstalk |
| 1 | 7.3×10^{-4} | 6.5×10^{-3} |
| 2 | 8.0×10^{-5} | 4.0×10^{-3} |
| 3 | 3.0×10^{-5} | 2.0×10^{-3} |
| 4 | 0 | 1.3×10^{-3} |
| 5 | 0 | 1.0×10^{-3} |
| 6 | 0 | 7.5×10^{-4} |

4.2.3.2 Effect of Booster Amplifier Gain

The gain of booster OA G_b affects the maximum transmission distance offered by the interconnect while keeping the receiver BER less than the threshold level ($= 4.5 \times 10^{-3}$). Many simulation tests are performed to determine the dependence of L_{\max} on G_b . In each test, the value of G_b is fixed while the interconnect length L is increased and the associated increased BER, $BER(L)$, is recorded. The maximum reach L_{\max} corresponds to the value of L which makes $BER(L) = BER_{th}$. Summary of the simulation results are depicted graphically in Fig. 4-4 where the values of L_{\max} are given for different levels of amplifier gain. The results are reported for both absence and presence of -20 dB crosstalk. Note that L_{\max} increases almost linearly with G_b for both cases with a slope ≈ 5 km/dB. This value corresponds to $1/\alpha$ where $\alpha = 0.2$ dB/km which is the value of the loss parameter of the MCF used in the simulation. Thus 1 dB increasing in the amplifier gain supports 5 km extra interconnect length.

4.3 Effect of Number of Channels, Number of Cores, and Bit Rate

This section addresses the effect of number of WDM multiplexed channels per core N_{ch} , number of cores N_c , and bit rate R_b on the performance of MCF-based OIC. The results are presented for two bit rates per channel, 320 and 640 Gbps.

4.3.1 (N_{ch} , N_c , 320) OIC

The first step is to investigate the performance of the 7-core OIC. Simulation results reveal that almost lossless transmission is achieved in the

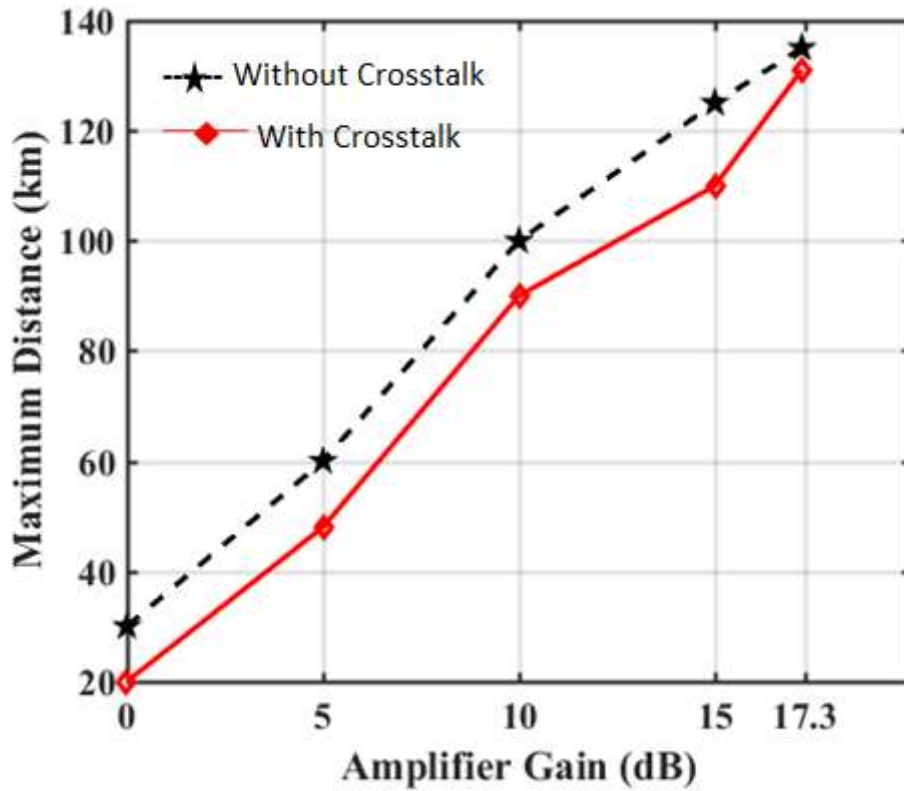


Figure 4-4 Effect of booster amplifier gain on the maximum transmission distance during absence of crosstalk and presence of -20 dB crosstalk for (7, 24, 320) OIC.

absence of crosstalk when the OIC is designed with 10 km length to support up to 96 WDM channels per core. The simulation is carried further to investigate the performance of a 10 km OIC implemented with 19 cores. The investigation indicates that this link can support the transmission of 96 channels per core when the $CT < -19.2$ dB. At $CT = -20$ dB, the received BER is 4.9×10^{-4} .

4.3.2 (N_{ch} , N_c , 640) OIC

This subsection investigates the transmission performance of MCF-OIC operating with 640 Gbps channel bit rate R_b . Assuming DP-16QAM

signaling, the symbol rate R_s is 80 GSps. Hence 100 GHz channel spacing Δf is used in the simulation. The frequency of the central WDM laser is kept at 193.1 THz while the frequencies of the other lasers spread around this value. All the multiplexers and demultiplexers are redesigned to incorporate the new value of Δf .

4.3.2.1 7-Core OIC

To illustrate the operation of the OIC under study, Fig. 4-5 shows the power spectra at different points of the system when $L=10$ km, $N_{Ch} = 24$,

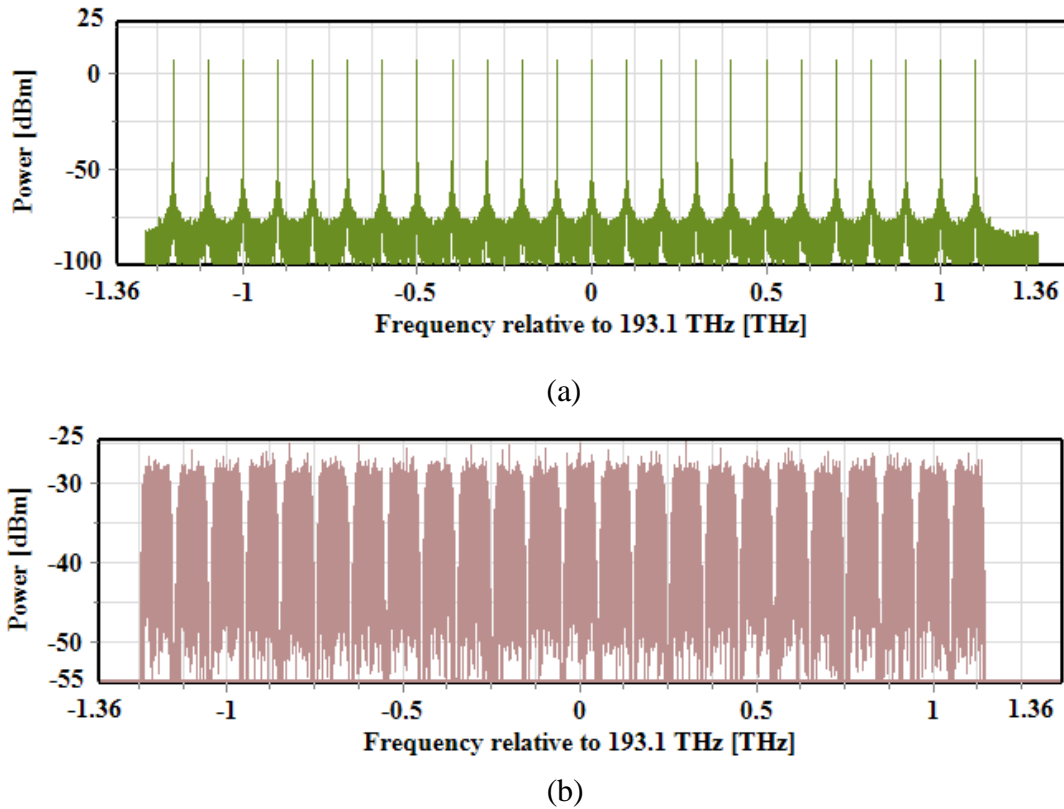
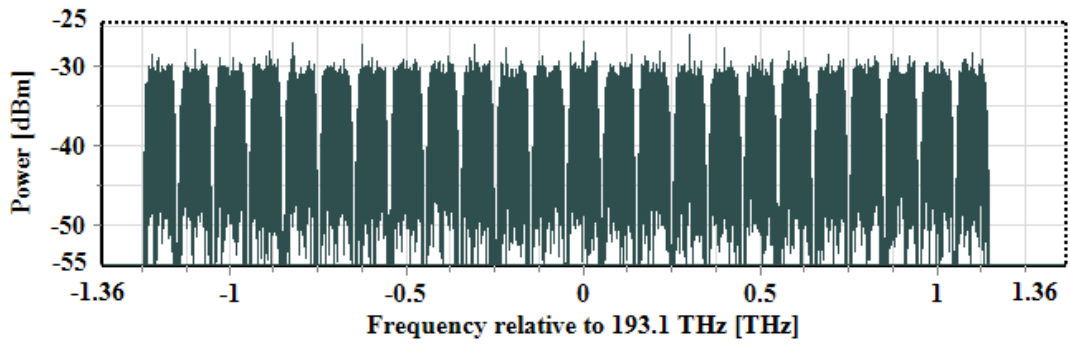
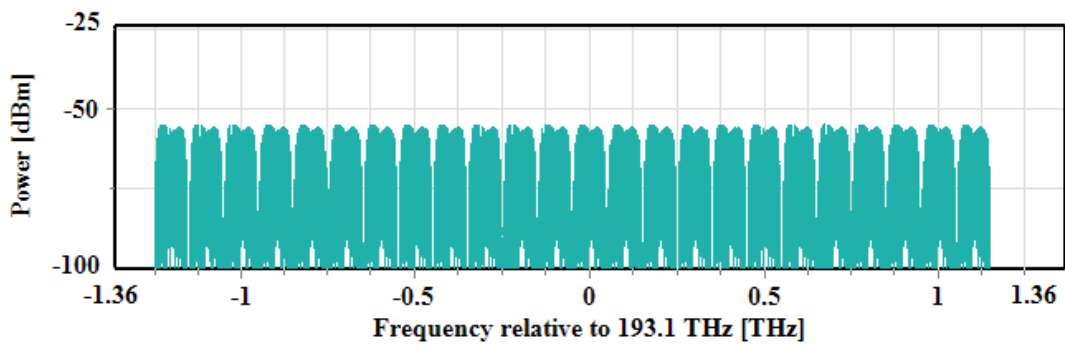


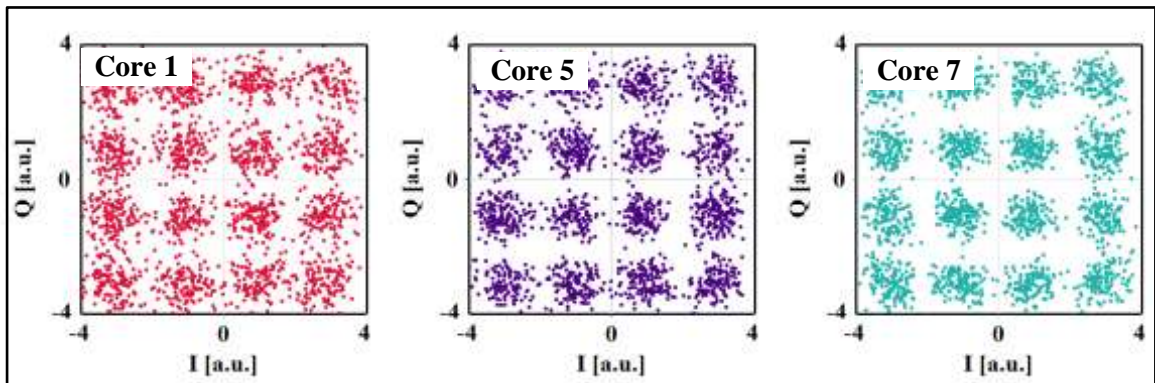
Figure 4-5 Optical spectra and constellation diagrams related to (7, 24, 640) system operating with -20 dB crosstalk (a) unmodulated WDM optical carriers (b) amplified SDM-WDM transmitter signal (c) optical signal after 10 km transmission (d) intercore crosstalk signal (e) constellation diagrams corresponding to Ch13 received in three different cores (core1, core5, and core7).



(c)



(d)



(e)

Figure 4-5 (Continued).

and $CT = -20$ dB. The receiver constellation diagrams for three cores (1, 5, 7) are also included in Fig 4.5e which gives an average BER of 2.0×10^{-3} .

Table 4-2 lists the maximum allowable crosstalk $(CT)_{\max}$ as a function number of multiplexed channel when $L = 10$ km. To be in the safe side and to ensure acceptable transmission performance independent of number of multiplexed channels, the crosstalk should be kept below -19 dB. It is noted that the 10 km-OIC offers almost lossless transmission for all values of N_{ch} considered here when CT is negligible.

Table 4-2 Maximum allowable crosstalk $(CT)_{\max}$ as a function number of multiplexed channels for a 7-core OIC operating with $R_b = 640$ Gbps.

| Number of Multiplexed Channels | Maximum Allowable Crosstalk (dB) |
|--------------------------------|----------------------------------|
| 24 | -18.2 |
| 48 | -17.7 |
| 72 | -18.5 |
| 96 | -17.8 |

4.3.2.2 19-Core OIC

Figure 4-6 shows the variation of BER with number of multiplexed channels for OIC designed with $L = 10$ km, $N_c = 19$, and $R_b = 640$ Gbps.

The results are presented for two cases, negligible crosstalk and $CT = -20$ dB. Investigating this figure reveals the following facts

- i. The BER performance degrades as the number of multiplexed channels increases.
- ii. In the absence of crosstalk, operating with $N_{ch} = 96$ does not achieve the required transmission performance.
- iii. Presence of -20 dB crosstalk increases the BER above BER_{th} even when $N_{ch} = 24$.

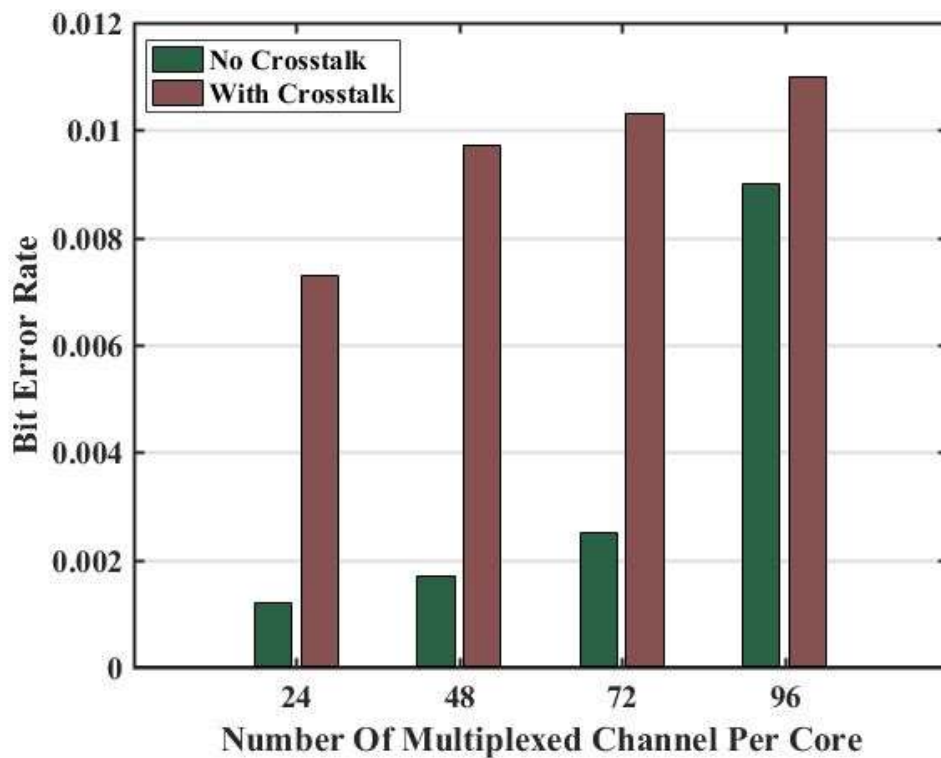


Figure 4-6 Variation of BER with number of multiplexed channels for 19-core, 10 km OIC operating with $R_b = 640$ Gbps.

It is obvious from the previous results that the 10 km OIC does not support the required BER level when it is designed with 19-core fiber and

$R_b = 640$ Gbps. Therefore, the OIC BER performance is then investigated when the interconnect length L is reduced below 10 km. Figure 4-7 illustrates the variation of BER with L when $N_{ch} = 24$ and $CT = -20$ dB. Clear constellation diagrams are obtained when $L = 6$ km.

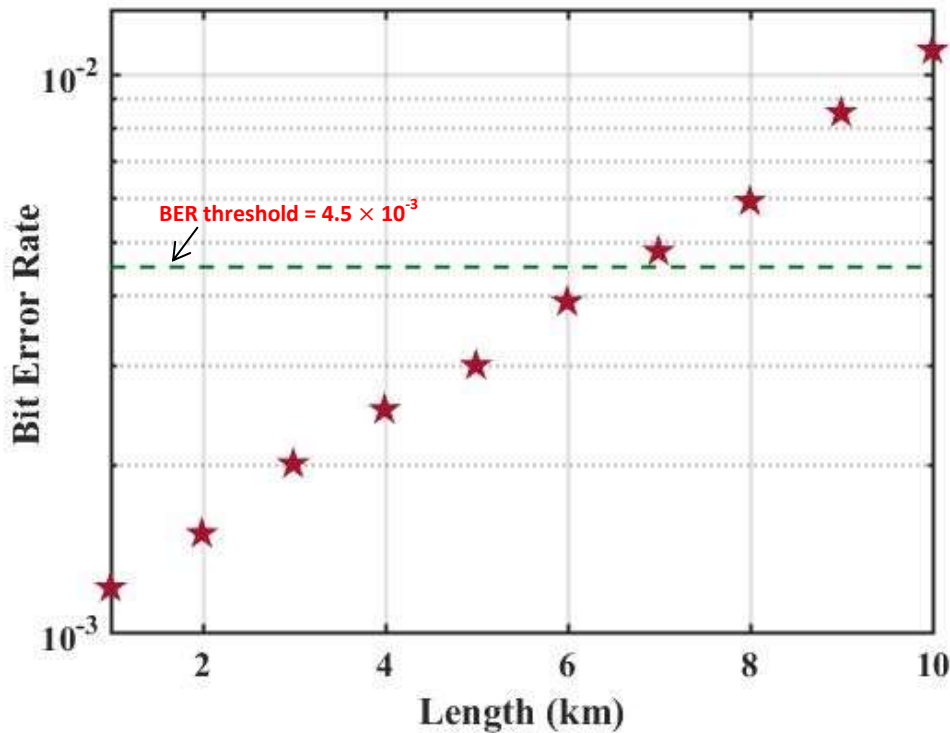
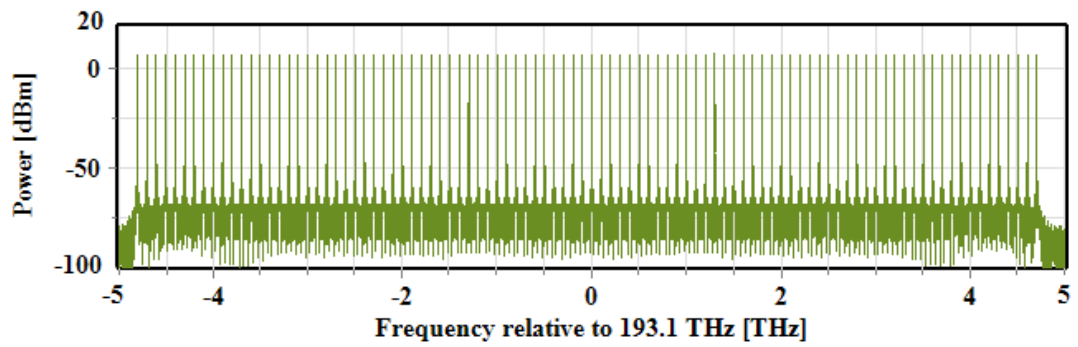
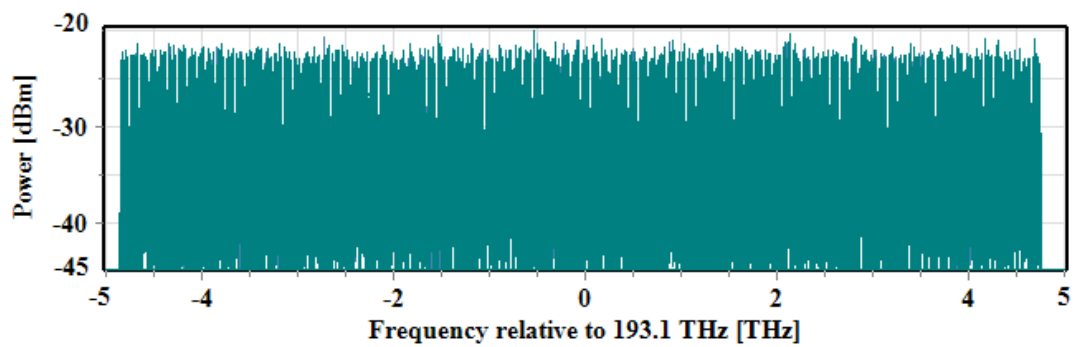


Figure 4-7 Variation of BER with transmission length for (19, 24, 640) OIC operating with -20 dB crosstalk.

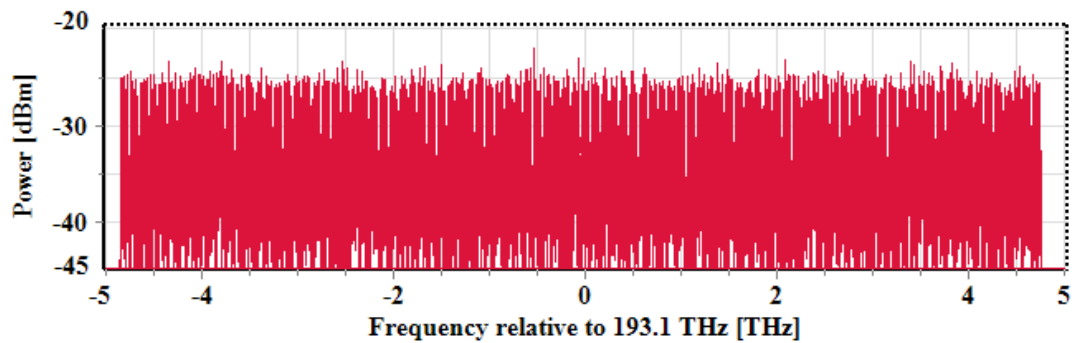
Simulation results indicate that the 19-core 5 km OIC can support the transmission of 96 channels per core when each channel carries 640 Gbps DP 16-QAM signals as shown in Fig. 4-8. The receiver BER is 8.0×10^{-4} and 3.0×10^{-3} in the absence and presence of -20 dB crosstalk, respectively. The corresponding $(CT)_{max}$ is -19.3 dB.



(a)

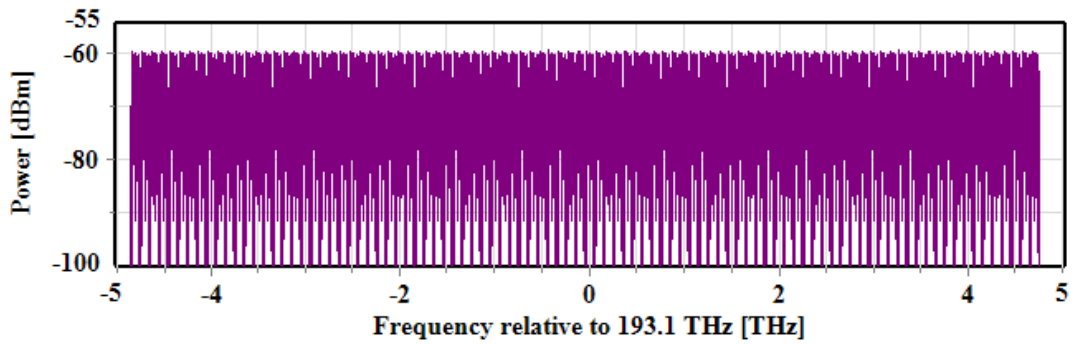


(b)

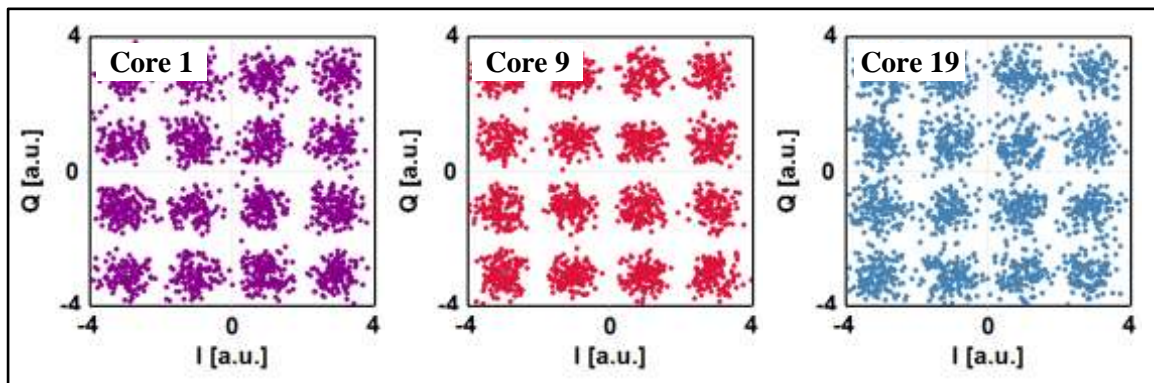


(c)

Figure 4-8 Optical spectra and constellation diagrams related to (19, 96, 640) OIC operating with -20 dB crosstalk (a) unmodulated WDM optical carriers (b) amplified SDM-WDM transmitter signal (c) optical signal after 5km transmission (d) intercore crosstalk signal (e) constellation diagrams corresponding to Ch49 received in three different cores (core1, core9, and core19).



(c)



(e)

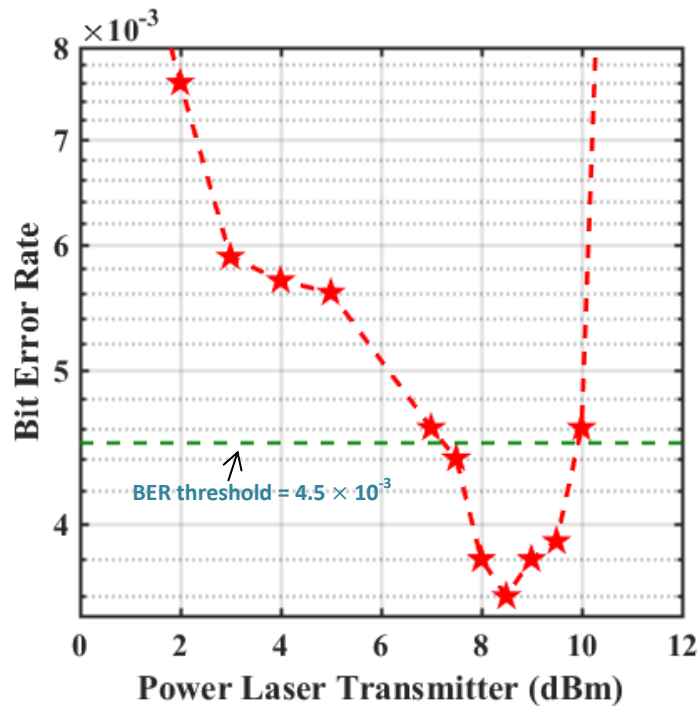
Figure 4-8 (Continued).

4.4 Effect of Fiber Nonlinear Optics

This section addresses the effect of fiber optic nonlinearity on the transmission performance of long-reach OIC designed with MCF-based SDM-WDM configuration. The nonlinearity comes from the dependence of core fiber refractive index “ n ” on the optical intensity “ I ” passing through it via Kerr-effect relation ($n(I) = n_0 + n_2 I$) [22]. In the simulation, the core low-intensity refractive index n_0 and nonlinear refractive index coefficient n_2 are set to 1.47 and $2.6 \times 10^{-20} \text{ m}^2/\text{W}$, respectively, at 193.1 THz frequency.

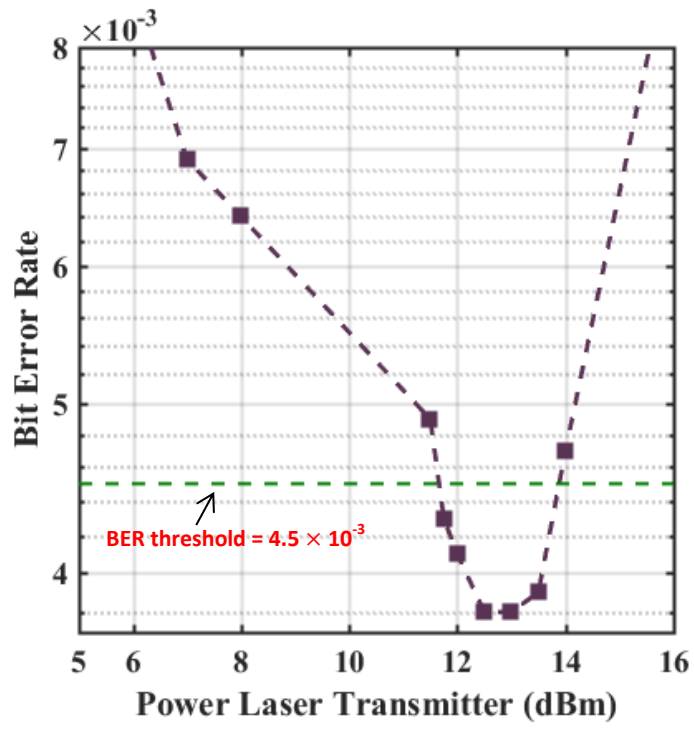
Simulation results are presented for 3-span OIC with each span consists of 100 km MCF followed by cascaded with 20 dB OA to compensate the fiber loss. The OIC carries 24-channel 320 Gbps DP 16-QAM signal per core.

Figures 4-9a-c show the dependence of received BER on the laser transmitter power P_{LT} for OICs designed with 7, 19, and 37 cores.

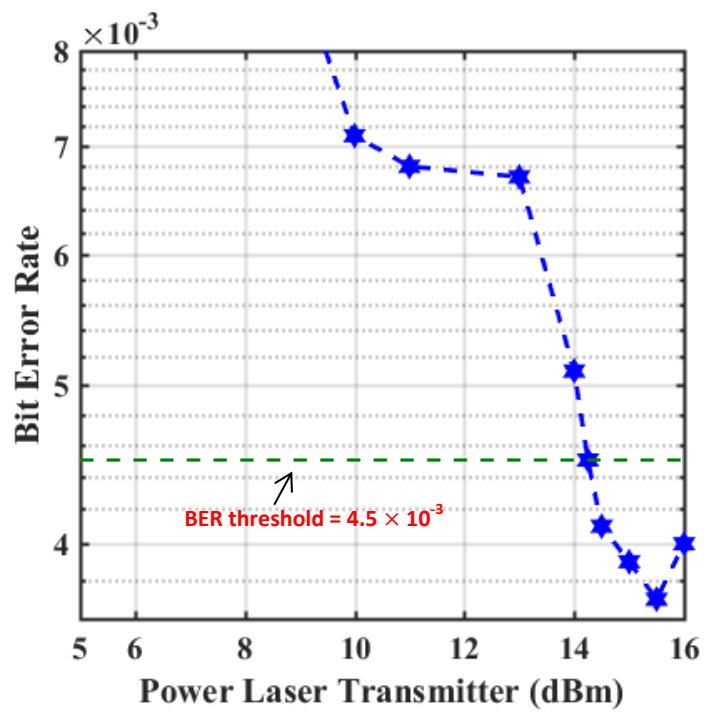


(a)

Figure 4-9 Dependence of BER on the power laser transmitter when 320 Gbps, DP 16-QAM channel signaling, three 100 km spans, and $N_{ch} = 24$ are assumed for (a) 7-core OIC.(b) 19-core OIC (c) 37-core OIC.



(b)



(c)

Figure 4-9 (Continued).

Table 4-3 summarizes the main results acquisitioned from Fig. 4-9 where the minimum and optimal values of P_{LT} , $(P_{LT})_{min}$ and $(P_{LT})_{opt}$, respectively, are reported for the three numbers of core. Here, $(P_{LT})_{min}$ denotes the minimum value of laser transmitter power P_{LT} which ensures received BER = BER_{th} . Furthermore, $(P_{LT})_{opt}$ indicates the value of P_{LT} which gives minimum BER. Investigating the results in Table 4-3 reveals the following fact. Going from 7-core design to 19-core and 37-core counterparts will increase both $(P_{LT})_{min}$ and $(P_{LT})_{opt}$ by 4.5 and 7.0 dB, respectively. These values are to be compared with $10\log(19/7) = 4.34$ dB and $10\log(37/7) = 7.23$ dB, respectively.

Table 4-3 Dependence of $(P_{LT})_{min}$ and $(P_{LT})_{opt}$ on number of cores for 24-channel per core, 320 Gbps, DP 16-QAM channel signaling, three 100 km spans, and $N_{ch} = 24$ OIC.

| Number of Cores | $(P_{LT})_{min}$ (dBm) | $(P_{LT})_{opt}$ (dBm) |
|-----------------|------------------------|------------------------|
| 7 | 7.25 | 8.5 |
| 19 | 11.75 | 13.0 |
| 37 | 14.25 | 15.5 |

To check if the OIC BER performance degradation that occurs when $P_{LT} > (P_{LT})_{opt}$ is due to fiber nonlinear optics, the transmission performance is recorded again when the fiber nonlinearity parameters n_2 is set to zero through the simulation. Figure 4-10 displays the variation of BER with P_{LT} for 7-core OIC. It is noted that BER decreases continuously with increasing P_{LT} . Furthermore, the simulation with $n_2 = 0$ yields a received BER

1.9×10^{-3} , 3.0×10^{-3} , 3.9×10^{-3} , and 4.9×10^{-3} when the 7-core OIC is designed with 3, 4, 5, and 6 spans, respectively.

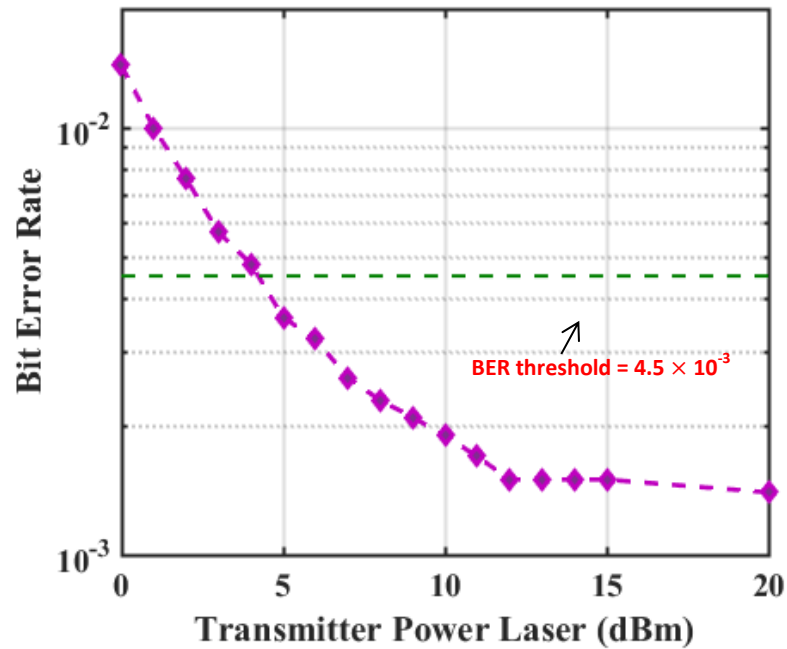


Figure 4-10 Variation of BER with transmitter power laser for 3×100 km, 7-cor, $R_b = 320$ Gbps, and $N_{ch} = 24$ OIC operating in the absence of nonlinearity.

CHAPTER FIVE

Conclusions and Suggestions for Future Work

5.1 Conclusions

The transmission performance of Tbps optical interconnects incorporating MCF-based SDM-WDM technique has been investigated in the presence of intercore crosstalk. The investigation has focused on the key roles played by : number of cores N_c , number of WDM channels N_{ch} , and bit rate per channel R_b . Simulation results have been reported for $R_b = 320$ and 640 Gbps DP 16-QAM signaling. For the purpose of comparison, the performance of single-core OICs designed for single-channel or WDM system transmission have been also investigated using $R_b = 320$ Gbps. The investigation reveals the following main conclusions

- (i) In the absence of booster amplifier, the single-core single-channel OIC can support 195 km transmission when the transmitter laser power $P_{LT} = 5$ dBm. Increasing P_{LT} from 0 to 10 dBm will increase the transmission reach L_{max} by 45 km. As the number of WDM channels N_{ch} increases, L_{max} decreases for the same value of P_{LT} due the effect of fiber nonlinearity.
- (ii) Homogenous MCF designed with $35 \mu m$ core pitch, less than $3.5 \times 10^{-3} m^{-1}$ coupling coefficient, and less than 50 mm bending radius is more suitable for short and medium-reach OICs operating with negligible crosstalk (< -20 dB).
- (iii) A 10 km 19-core OIC can support the transmission of 580 Tbps data when it operates with $N_{ch} = 96$ and $R_b = 320$ Gbps.

- (iv) A 10 km 7-core OIC can support the transmission of 430 Tbps data, ($N_{\text{ch}} = 96$ and $R_b = 640$ Gbps). This is to be compared with 1160 Tbps when the interconnect is redesigned with $L = 5$ km and $N_c = 19$.
- (v) The effect of laser linewidth on OIC performance is more pronounced in the presence of crosstalk.
- (vi) The crosstalk level CT should be kept below -18 dB to ensure satisfactory transmission over 10 km-OIC. This threshold level varies slightly with N_c , N_{ch} , and R_b .
- (vii) The effect of fiber nonlinear optics on the transmission performance of long OIC becomes more pronounced when large number of WDM channels and high value of P_{LT} are used. The optimum value of P_{LT} , that gives maximum reach, increases with number of fiber cores.

5.2 Suggestion for Future Work

The work in this thesis opens the way to new research issues to be addressed in the future such as

- (i) Investigating the transmission performance of MCF-based SDM OIC when each core supports few modes rather than single mode. Although such OIC can support higher transmission capacity but its operation is affected by two types of crosstalk, namely intercore and intercore (i.e., intermodal) crosstalk.
- (ii) The modulation format used in this work is DP 16-QAM. Extending the work to include other higher-order modulations formats such as DP 32-QAM and DP 64-QAM is an interesting point. The effect of

intercore crosstalk is expected to be higher when compared with DP 16-QAM signal and this issue should be addressed in details.

- (iii) Using optical orthogonal frequency-division multiplexing technique (OFDM) to support longer transmission for MCF-based SDM OIC. In such technique, the data is used to modulate many subcarriers at the electrical domain and the resultant waveform is used to modulate the optical carrier. The optical OFDM reduces the effect of OIC dispersion and enables low-cost electrical equalization at the receiver side.

REFERENCES

- [1] **Y. Loussouarn, E. Pincemin, S. Gauthier, Y. Chen, W. Yuan, Y. Hong, X. Wei, and Z. Dejiang**, “Single-carrier and multi-carrier 400 Gbps transmission with multi-rate multi-format real-time transceiver prototypes,” *IEEE Journal of Lightwave Technology*, vol. 37, no. 2, pp. 524–537, January 2019.
- [2] **B. Buscaino, B. Taylor, and J. Kahn**, “Multi-Tb/s-per-fiber coherent o-Packaged optical interfaces for data center switches,” *IEEE Journal of Lightwave Technology*, vol. 37, no. 13, pp. 3401–3412, July 2019
- [3] **T. Mizuno, H. Takara, A. Sano, and Y. Miyamoto**, “Dense Space-Division Multiplexed Transmission,” vol. 34, no. 2, pp. 582–592, January 2016.
- [4] **Y. Wakayama, D. Soma, S. Beppu, S. Sumita, K. Igarashi, and T. Tsuritani**, “266.1-Tbit/s transmission over 90.4-km 6-mode fiber with inline dual C+L-band 6-mode EDFA,” *IEEE Journal of Lightwave Technology*, vol. 37, no. 2, pp. 404–410, January 2019.
- [5] **H. Takara, H. Ono, Y. Abe, H. Masuda, K. Takenaga, S. Matsuo, H. Kubota, K. Shibahara, T. Kobayashi, and Y. Miaymoto**, “1000-km 7-core fiber transmission of 10 x 96-Gb/s PDM-16QAM using Raman amplification with 6.5 W per fiber,” *Optics Express*, vol. 20, no. 9, pp. 10100-10105, April 2012.
- [6] **J. Sakaguchi, W. Klaus, Y. Awaji, N. Wada, T. Hayashi, T. Nakanishi, T. Taru, T. Takahata, and T. Kobayashi**, “228-spatial-channel bi-directional data communication system enabled by 39-core 3-mode fiber,” *IEEE Journal of Lightwave Technology*, vol. 37, no. 8, pp. 1756–1763, April 2019.
- [7] **T. Zami, B. Lavigne, I. Ruiz, M. Bertolini, Y. Kao, O. Pardo, M. Lefrancois, F. Pulka, S. Chandrasekhar, J. Cho, X. Chen, D. Che, E. Burrows, P. Winzer, J. Pesic, and N. Rossi**, “Simple self-optimization of WDM networks based on probabilistic constellation shaping,” *Jornal of Optical Communications and Networking*, vol. 12, no. 1, pp. A82–A94, October 2019.

- [8] **S. Rommel, D. Perez-Galacho, J. Fabrega, R. Munoz, S. Sales, and I. Monroy**, “High-capacity 5G fronthaul networks based on optical space division multiplexing,” *IEEE Transaction on Broadcasting*, vol. 65, no. 2, pp. 434–443, June 2019.
- [9] **J. Gene and P. Winzer**, “A universal specification for multicore fiber crosstalk,” *IEEE Photonics Technology Letters*, vol. 31, no. 9, pp. 673–676, May 2019.
- [10] **C. Kachris, K. Bergman, I. Tomkos**, " *Optical Interconnects for Future Data Center Networks*", 1st Edition , Springer , 2013.
- [11] **Neophotonics**, “Understanding data center interconnect: Intra-data center.” <https://www.neophotonics.com/understanding-intra-data-center-interconnect/> (accessed January 11, 2020).
- [12] **R. Lin, J. Kerrebrouck, X. Pang, M. Verplaetse, O. Ozolins, A. Udalcovs, L. Zhang , L. Gan, M.Tang , S. Fu , R. Schatz, U. Westergren, S. Popov, D. Liu, W. Tong , T. Keulenaer, G. Torfs, J. Bauwelinck, X. Yin and J. Chen**, “Spatial division multiplexing for optical data center networks”, 2018 International Conference on Optical Network Design and Modeling (ONDM), pp. 239-241, 2018.
- [13] **D. Butler, M. Li, S. Li, Y. Geng, R. Khrapko, R. Modavis, V.Nazarov, and A. Koklyushkin**, “Space division multiplexing in short reach optical interconnects”, *IEEE Journal of Light wave Technology*, vol. 35, no. 4, pp. 677- 682, February 2017.
- [14] **H. Yuan, M. Furdek, A. Muhammad, A. Saljoghei, L.Wosinska, and G. Zervas**, “Space-division multiplexing in data center networks on multi-core fiber solutions and crosstalk-suppressed resource allocation“, *IEEE Journal of Optical Communication Networks*, vol. 10, no. 4, pp. 272-287, April 4, 2018.
- [15] **H. Yuan , A. Saljoghei , A. Peters , and G. Zervas**, “Comparison of SDM-WDM based Data Center Networks with equal/unequal core pitch Multi-Core Fibers”, *IEEE Optical Society of America*, 2018 .
- [16] **L. Yan, M. Fiorani, A. Muhammad, M. Tornatore, E. Agrell, and L. Wosinska**, “Network performance trade-off in modular data centers with optical spatial division multiplexing,” *Journal of Optical Communications and Networking*, vol. 10, no. 9, pp. 796–808, September 2018.

- [17] **L. Zhang, J. Chen, E. Agrell, R. Lin, and L. Wosinska**, “Enabling technologies for optical data center networks: Spatial division multiplexing,” *IEEE Journal of Lightwave Technology*, vol. 38, no. 1, pp. 18–30, 2020.
- [18] **J. Mendinueta, S. Shinada, Y. Hirota, R. Luis, H. Furukawa, and N. Wada**, “Converged inter/intradata center optical network with packet super-channels and 83.33 Tb/s/port,” *IEEE Journal of Lightwave Technology*, vol. 37, no. 2, pp. 571–578, 2020.
- [19] **I. Abdullah, and M. Maher**, “Design of space division multiplexing with six polarized and multiplexed modes of PDM/DWDM system using multimode splicer enabling gray mapping and MIMO equalizer,” *International Journal of Computer Science and Mobile Applications*, vol. 4, no. 9, pp. 4–13, September 2016.
- [20] **E. Hamed, M. Munshid, and J. Hmood**, “Impact of fiber nonlinearity on the performance of mode division multiplexing systems,” *Iraqi Journal of Computers Communication and Control & Systems Engineering*, vol. 19, no. 2, pp. 41–49, April 2019.
- [21] **M. Abdulzahra, A. Shamman, O. Ghayyib, and A. Almhanna**, “Transmission of SDM/DWDM system over 1500-KM with 16 spatial and polarized modes over few-mode fiber enabling advanced DSP algorithms,” *International Research Journal of Innovations in Engineering and Technology*, vol. 3, no. 1, pp. 9–13, January 2019.
- [22] **G. Agrawal**, “*Nonlinear Fiber Optics*”, 6th edition, Academic Press, 2019.
- [23] **L. Binh** “*Optical Fiber Communication Systems with Matlab and Simulink Models*”, Second Edition, CRC Press, 2014.
- [24] **G. Agrawa**, “*Fiber Optic Communication Systems*”, 4th Edition, Wiley, 2010.
- [25] **Nokia-Siemens Networks**, “Space division multiplexing: A new milestone in the evolution of fiber optic communication”, White paper, 2013. http://modegap.eu/wpcontent/uploads/2013/03/Nokia_Siemens_Networks_optical_future_paper_14_03_13.pdf (accessed July 20, 2019).
- [26] **A. Paradisi, R. Figueiredo, A. Chiuchiarelli, E. Rosa**, “*Optical Communications- Advanced Systems and Devices for Next Generation*”

Networks ", 1st Edition , Springer , 2019.

- [27] **D. Kakati and S. Arya**, "A full-duplex pilot-assisted DP-16-QAM CO-OFDM system for high-speed long-haul communication," International Conference on Innovations in Electronics, Signal Processing and Communication , India, November 2019.
- [28] **Y. Awaji**, "Review of space-division multiplexing technologies in optical communications," IEICE Transactions on Communications, vol. E102-B, no. 1, pp. 1–16, January 2019.
- [29] **G. Chen, C. Chow, C. Yeh, C. peng, P. Guo, J. Tsai, M. Cheng, Y. Tong, and H. Tsang**, "Mode-division-multiplexing (MDM) of 9.4-Tbit/s OFDM signals on silicon-on-insulator (SOI) platform," IEEE Access, vol. 7, pp. 129104–129111, September 2019.
- [30] **R. Soeiro, T. Alves, and A. Cartaxo**, "Inter-core crosstalk in weakly coupled MCFs with arbitrary core layout and the effect of bending and twisting on the coupling coefficient," Optics Express, vol. 27, no. 1, pp. 74-91, January 2019.
- [31] **A. Elfiqui, A. Ali, Z. El-Sahn, K. Kato, and H. Shalaby**, "Theoretical analysis of long-haul systems adopting mode-division multiplexing," Optics Communication, vol. 445, pp. 10–18, April 2019.
- [32] **G. Saridis, D. Alexandropoulos, G. Zervas, and D. Simeonidou**, "Survey and evaluation of space division multiplexing: From technologies to optical networks," IEEE Communications Surveys and Tutorials, vol. 17, no. 4, pp. 2136–2156, August 2015.
- [33] **Z. Di, Z. Yang, Y. Liu, G. Peng, L. Zhang, G. Li**, "Measurement of Principal Modes in Few-mode Fibers by S2 Method" IEEE Photonics Journal, pp. 1–1, March 2020.
- [34] **T. Hayashi and T. Nakanishi**, "Multi-core optical fibers for the next-generation communications," Sei Technical Review, no. 86, pp. 23–28, 2018.
- [35] **K. Saitoh, M. Koshihara, K. Takenaga, and S. Matsuo**, "Crosstalk and core density in uncoupled multicore fibers," IEEE Photonics Technology Letters, vol. 24, no. 21, pp. 1898–1901, November 2012.

- [36] **T. Mizuno, K. Shibahara, F. Ye, Y. Sasaki, Y. Amma, K. Takenaga, Y. Jung, K. Pulverer, H. Ono, Y. Abe, M. Yamada, K. Saitoh, S. Matsuo, K. Aikawa, M. Bohn, D. Richardson, Y. Miyamoto, and T. Morioka**, “Long-haul dense space-division multiplexed transmission over low-crosstalk heterogeneous 32-core transmission line using a partial recirculating loop system,” *IEEE Journal of Lightwave Technology*, vol. 35, no. 3, pp. 488–498, February 2017.
- [37] **B. Puttnam, R. Luís, G. Rademacher, A. Alfredsson, W. Klaus, J. Sakaguchi, Y. Awaji, E. Agrell, and N. Wada**, “Characteristics of homogeneous multi-core fibers for SDM transmission”, *APL Photonics*, vol. 4, no. 2, 2019.
- [38] **T. Alves and A. Cartaxo**, “Decorrelation bandwidth of intercore crosstalk in weakly coupled multicore fibers with multiple interfering cores,” *IEEE Journal of Lightwave Technology*, vol. 37, no. 3, pp. 744–754, February 2019.
- [39] **K. Saitoh and S. Matsuo**, “Multicore fibers for large capacity transmission,” *Nanophotonics*, vol. 2, no. 5–6, pp. 441–454, August 2013.
- [40] **J. Speidel**, “Introduction to digital communications”, 1st Edition, Springer, 2019.
- [41] **L. Binh**, “Advanced digital optical communications”, 2nd Edition, CRC Press, 2019.
- [42] **N. Suzuki, H. Miura, K. Matsuda, R. Matsumoto, and K. Motoshima**, “100 Gb/s to 1 Tb/s based coherent passive optical network technology,” *IEEE Journal of Lightwave Technology*, vol. 36, no. 8, pp. 1485–1491, April 2018.

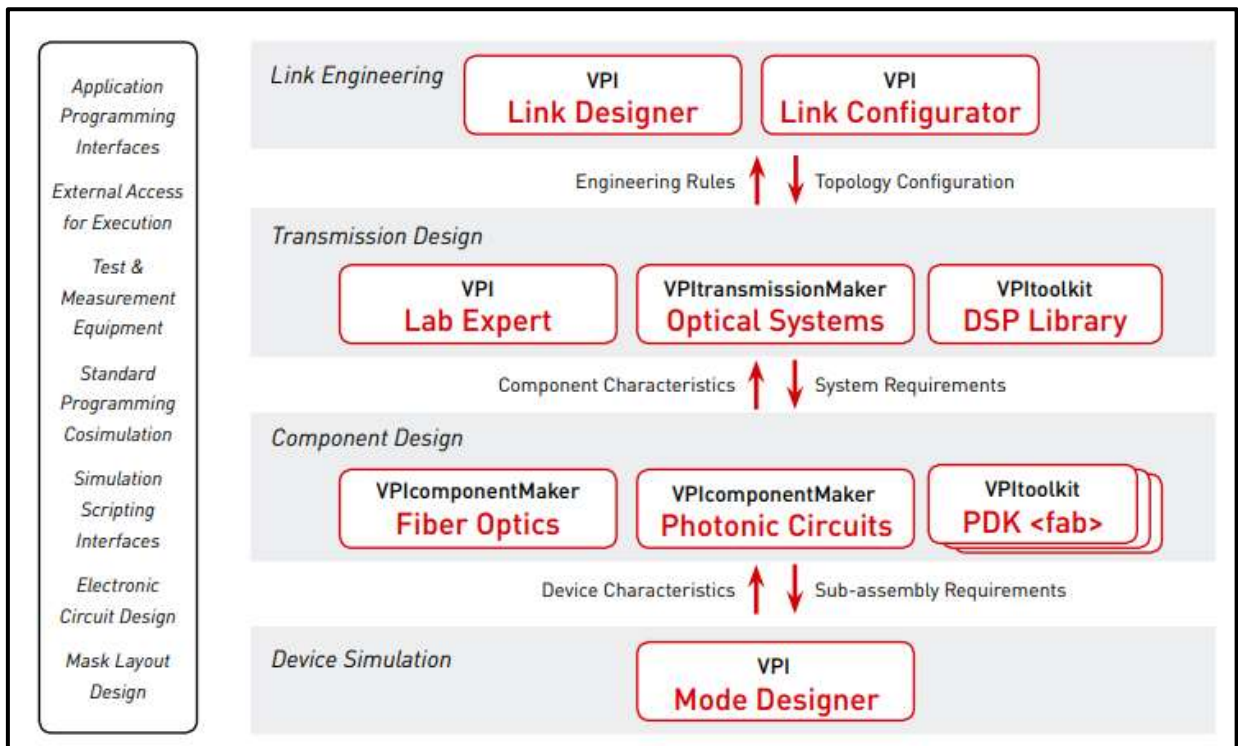
APPENDICES

Appendix A

VPIphotonics Software

VPIphotonics™ – Overview

VPIphotonics sets the industry standard for end-to-end photonic design automation comprising design, analysis and optimization of components, systems and networks. VPIphotonics team provide professional simulation software supporting requirements of integrated photonics, optoelectronics and fiber optics applications, optical transmission system and networks, as well as link engineering and equipment configuration. A wide range of interfaces to the tools used by peers, third party software, laboratory equipment, and existing databases are available.



Design and Engineering Solutions

VPIphotonics provides comprehensive Photonic Design Automation (PDA) solutions for 20+ years comprising of design methodologies, software tools and services used to engineer complex photonic networks and products. VPIphotonics software solutions embed expert knowledge in flexible working environments supporting many applications in various fields of operation. VPIphotonics brings efficiency gains as it supports a streamlined design process:

- ✓ Enable collaborative designs via supply chains
- ✓ Stimulate innovation by expanding available resources
- ✓ Reduce the need for physical experimentation
- ✓ Capture and distribute knowledge of design processes
- ✓ Establish and support robust decision-making processes

i. Link Designer

VPIlinkDesigner™ is a cost-effective, easy to use tool which enables fast and optimum network design and provisioning for those who design and configure links in optical networks and sub-networks.

ii. Link Configurator

VPIlinkConfigurator™ provides an intuitive graphical interface and powerful algorithms for optical network engineering including automatic equipment placement and a thorough system wide performance assessment.

iii. Optical Systems

VPItransmissionMaker™ Optical Systems accelerates the design of new photonic systems and subsystems for short-range, access, metro and long-haul transmission systems. Further, it supports the assessment of

technology upgrade and component substitution strategies that are to be developed for existing network plants.

iv. Lab Expert

VPIlabExpert™ addresses the specific requirements of experimentalists for data pre- and post-processing and signal analysis functions for optical communications. It reduces efforts in the laboratory by applying ready-to-use advanced functionalities and virtualizing lab equipment through the emulation of component characteristics.

v. Photonic Circuits

VPIcomponentMaker™ Photonic Circuits is a simulation and design environment for photonic integrated circuits (PICs). It provides advanced device libraries integrated with a scalable time-and-frequency-domain simulation framework for fast and accurate modeling of large-scale PICs with a mix of photonic, electrical and optoelectronic devices.

vi. Fiber Optics

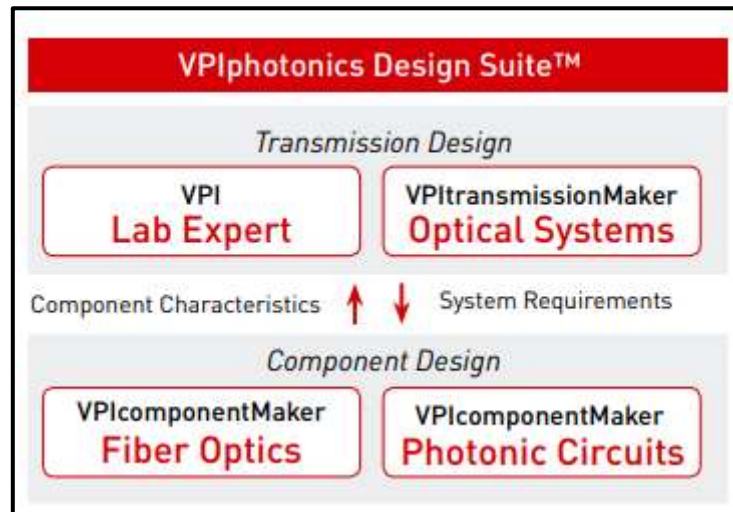
VPIcomponentMaker™ Fiber Optics provides professional means for modeling, optimization and design of fiber-based optical devices such as doped-fiber, Raman and parametric amplifiers, continuous-wave and pulsed optical fiber sources, optical signal processing for telecommunication, high-power and ultrafast applications.

vii. Mode Designer

VPImodeDesigner™ is a versatile simulation framework for the analysis and optimization of integrated photonic waveguides and optical fibers. This design tool offers full-vectorial finite-difference mode solvers for the accurate and efficient calculation of guided and leaky modes and their properties.

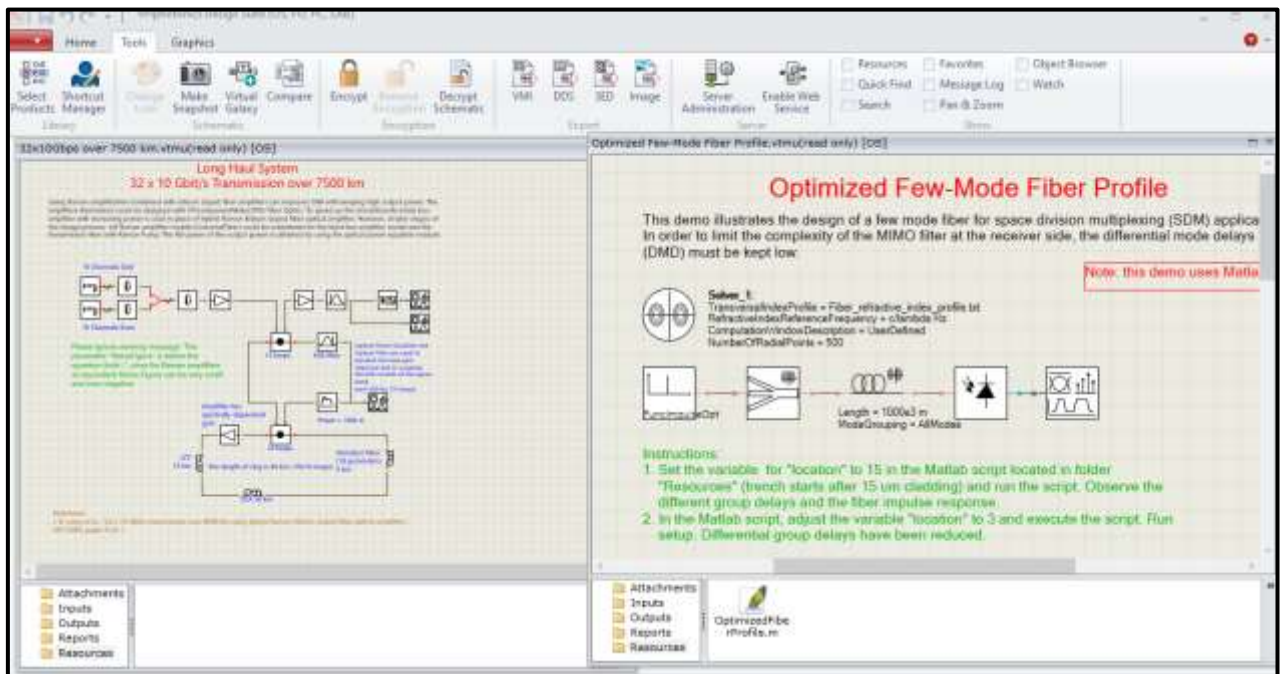
Design Suit

VPIphotonics Design Suite™ embeds expert knowledge from our component and transmission design tools in one shared, flexible software environment to support requirements in design, analysis and optimization providing you with the most powerful numerical algorithms tailored for your applications.



The flexible and intuitive graphical user interface of VPIphotonics Design Suite delivers access to sophisticated component, subsystem and photonic system design functions. VPIphotonics supports decision processes along the design chain of optical equipment, from conceptual studies to yield optimization. Comprehensive libraries with hundreds of demonstrations and sample equipment, system and network models accelerate learning and the execution of design tasks. Design process tools such as Interactive Simulations, (Tuning, Sweeps, Optimization, Monte-Carlo), Macros, Wizards, Simulation Scripting, Parameter Estimators, and third-party interfaces make VPIphotonics' products the backbone of the photonics simulation world. Parameters for any schematic or model can be managed with interactive controls or driven by sweeps and random number generators. The outputs of controls and sweeps can be combined and manipulated with

mathematical expressions, and then applied to multiple parameters. Simulations can be run in parallel on multiple cores or farmed out to remote machines. They can be driven by a flexible simulation scripting language to control large-scale numerical experiments. Proprietary content of subsystems can be encrypted and password-protected, so that simulations of proprietary models can be executed by end users, while the underlying schematics are locked from view. Data file attachments can be encrypted so that unauthorized users are unable to read the file.



Data Visualization & Analysis - VPIphotonicsAnalyzer™

VPIphotonicsAnalyzer™ establishes a universal framework for data display and analysis. It allows maximum freedom in the display, arrangement, export and analysis of simulation results from VPItransmissionMaker, VPIcomponentMaker, VPIlabExpert and third-party software. VPIphotonicsAnalyzer framework provides visualizers and analyzers that

accurately represent laboratory Test & Measurement equipment for detailed results display, component characterization and system performance analysis functions. The LinkAnalyzer, for instance, offers means for tracking signal properties along the fiber link without the need to run long-lasting simulations, and evaluating them versus position, distance or frequency.



- Multi-input optical, electrical oscilloscope
- Eye plots featuring color-grading, BER contours and customizable masks
- Optical spectrum analyzer with Stokes, phase, delay and dispersion plots
- RF spectrum analyzer with phase and delay
- Numerical 1D, 2D, 3D analysis with plot or text display and histogram mode

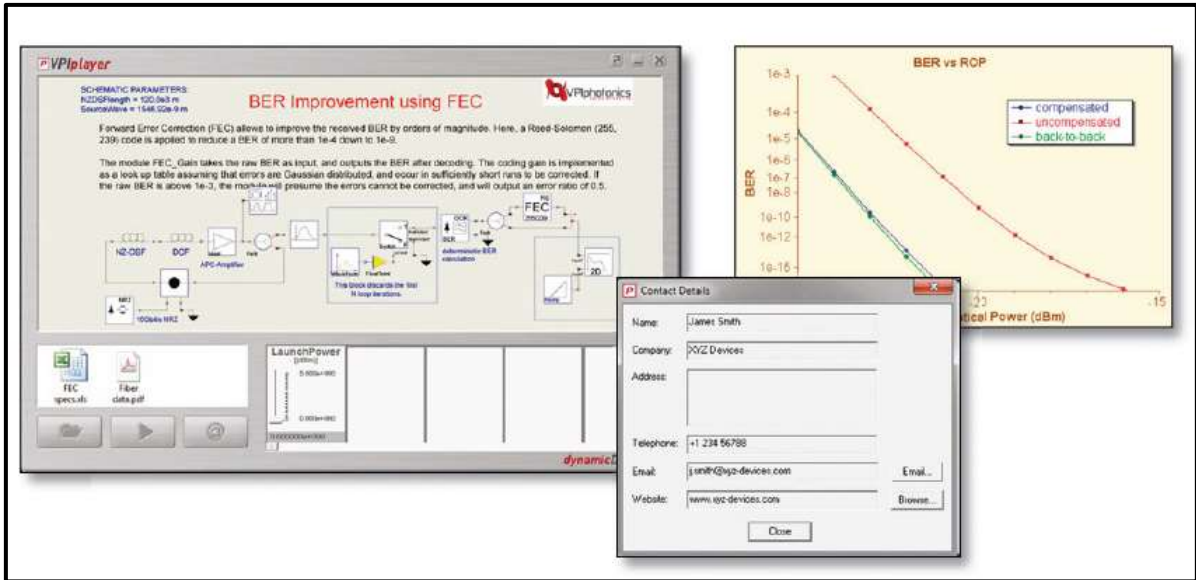
- Link Analysis (GVD, noise/distortion/signal power, Kerr, DGD, OSNR-, Q-, BER-limit vs distance, frequency, time)
- Constellations, CATV characterization
- Optical amplifier test set with gain, NF, BER
- Two-port electrical signal analyzers
- BER estimators for various receiver architectures
- Poincaré sphere with markers
- PMD test set (PSP, PCD, DGD, Jones)
- Laser characterization tools

VPIplayer™ & Interfaces to Third Parties

VPIplayer™

The communications tool provides a format to exchange photonic designs by running complex simulations while protecting intellectual properties of the owner. VPIplayer empowers engineers to present their ideas to colleagues and customers who have less technical knowledge, and no need for detailed design and simulation software. It is downloadable for free from www.VPIphotonics.com/Tools/VPIplayer.

VPIplayer runs a DynamicDataSheet™ (DDS), which captures product specifics as a simulation schematic generating results on data visualizers and analyzers. A DDS can be created by exporting a simulation setup from VPItransmissionMaker / VPIcomponentMaker. Your company logo, contact details and supporting information can be included. Interactive settings allow users to adjust parameters via predefined sliders.



Third-Party Interfaces

Cosimulation allows parts of a simulation schematic to be modeled using third-party or in-house code. Live interfaces to MATLAB, Python, C++ and any software supporting the COM interface are provided, so simulations seamlessly interact with models in these formats. Vice versa, the Simulation Engine Driver (SED) provides access to the simulation engine of VPIphotonics Design Suite for external systems and third-party tools. Electronic circuit models from Keysight’s Advanced Design System (ADS) can be called and their parameters controlled directly from VPIphotonics’ design tools allowing to assess the performance of high-speed electronics in photonic link designs. VPIphotonics simulations can import data from component characterizations and systems measurements. Various interfaces exist; new formats can be defined using customizable Data Type Converters and Macros.

شكر وتقدير

اللهم لك الحمد حمداً أبلغ به رضاك وأودي به شكرك وأستوجب به المزيد من فضلك, اللهم صل على محمد وآله الطيبين الطاهرين وصحبه المنتجبين.

وانا أضع يدي على اللمسات الأخيرة في كتابة رسالتي هذه أرى من الوفاء أن أتقدم بجزيل الشكر والامتنان الى أستاذي المرابي الفاضل الدكتور رعد سامي فياض لما بذله من جهد متواصل ونصح وتوجيه مستمر من بداية مرحلة البحث وحتى اتمام هذه الرسالة. ومن الواجب والعرفان أن أتقدم بشكري وتقديري لعميد كلية الهندسة ورئيس قسم هندسة الحاسوب وجميع اعضاء قسم هندسة الحاسوب المحترمين لما قدموه من توجيهات سديدة وراء أغنت البحث.

كما واتقدم بالشكر الى من دفعني الى العلم وبه ازاد أفتخاراً قدوتي ومثلي الأعلى والدي العزيز , ولوالدي التي بوجودها اكسبتي قوة و بثت في روحي الامل وزرعت في نفسي الثقة عند كل خطوة. ثم اتوجه بالشكر الى أختي و أخوتي لما قدموه من دعم وتشجيع طيلة فترة دراستي.

والشكرموصول الى كل صديقاتي واصدقائي وكل من قدم النصح والمساعدة وكان معي سنداً وعوناً خلال انجاز هذا البحث.

الخلاصة

شهدت الاونة الاخيرة اهتماماً متزايداً بتصميم مراكز بيانات بروابط ضوئية ذات سعة عالية (OICs) لتلائم النمو المتزايد والكبير في حركة البيانات المراد معالجتها والمرتبطة بتطبيقات الوسائط المتعددة المتقدمة وانترنت الأشياء. يتطلب التصميم استخدام تقنيات تعدد ارسال مختلفة للتمكن من ارسال بيانات بمعدل تيرابايت في الثانية (Tbps). تتناول هذه الرسالة التحديات التي تواجه تصميم الـ OIC Tbps باستخدام الالياف المتعددة النواة (MCF) المدعومة بتقنية تعدد الأرسال بتقسيم الفضاء (SDM) وتقنية تعدد الأرسال بتقسيم الطول الموجي (WDM).

تم تصميم الرابط الضوئي SDM المستند إلى MCF وبناءؤه في بيئة برمجيات VPIphotonicsالنسخة (9.8) . كل نواة بصرية تدعم الأرسال في نظام الـ WDM حيث ان كل قناة تعمل بتقنية ثنائي الأستقطاب (DP) مع صيغة تضمين 16-QAM. وتم دراسة التداخل الحاصل بين الاشارات المرسله في النوى المتجاورة داخل الليف الضوئي لمعرفة تأثيره على كفاءة الأرسال في OIC نسبة الى عدد من المتغيرات تشمل عدد النوى N_c وعدد قنوات WDM لكل نواة N_{ch} و معدل البتات بكل قناة R_b وطول الليف الضوئي L , تم تسجيل نتائج المحاكاة باستخدام قيم R_b تساوي 320 و 640 جيجابت لكل ثانية و N_c يساوي 7 و 19 و N_{ch} يصل الى 96 قناة. تكشف النتائج أن L تساوي 10 و 5 كم من OICs المكونة من 19 نواة يمكن أن تدعم إرسال 96 قناة WDM لكل نواة تعمل مع R_b تساوي 320 و 640 جيجابت في الثانية على التوالي ، عند إبقاء مستوى التداخل المتبادل أقل من 20- ديسيبل ، لينتج سعة ارسال حوالي 580 و 1160 تيرابت في الثانية. التحقيق امتد ليشمل مسافات اطول من OICs المصممة من MCF متعدد الأجزاء الطولية و المعوض عن الخسارة. أظهرت النتائج أن تأثيرات الليف الضوئي اللاخطية تقلل من أداء الإرسال عندما تكون L و N_{ch} كبيرة وبالتالي يجب اختيار قيمة مثلى لقدرة ليزر المرسله لتحقيق أقصى مسافة ممكنة.



وزارة التعليم العالي والبحث العلمي
جامعة النهرين/ كلية الهندسة

تحسين أداء مراكز البيانات الضوئية باستخدام تقنيات مضاعفة تقسيم الفضاء

رسالة مقدمة

الى كلية الهندسة في جامعة النهرين

وهي جزء من متطلبات نيل شهادة ماجستير علوم

في

هندسة الحاسوب

من قبل

ساره كريم سالم

(بكالوريوس علوم في هندسة الحاسوب ٢٠٠٩ م)

١٤٤١ هـ

٢٠٢٠ م

ذو القعدة

تموز